FKG

Institute of
Oceanographic Sciences
Deacon Laboratory

INTERNAL DOCUMENT No. 344

Analysis of buoy motion package data

C H Clayson

1994

Natural Environment Research Council

INSTITUTE OF OCEANOGRAPHIC SCIENCES
DEACON LABORATORY

INTERNAL DOCUMENT No. 344

Analysis of buoy motion package data

C H Clayson

1994

Wormley
Godalming
Surrey GU8 5UB UK
Tel +44-(0)428 684141
Telex 858833 OCEANS G
Telefax +44-(0)428 683066

DOCUMENT DATA SHEET

AUTHOR	PUBLICATION DATE
CLAYSON, C H	1994

TITLE

Analysis of buoy motion package data.

REFERENCE

Institute of Oceanographic Sciences Deacon Laboratory, Internal Document, No. 344, 50pp. (Unpublished manuscript)

ABSTRACT

A Buoy Motion Package (BMP) was developed in early 1993 for the purpose of monitoring the motion of the Sonic Buoy during seakeeping trials. The sensors incorporated in the package gave sufficient information to derive the directional wave spectrum, assuming that the buoy was a good slope follower.

In the Autumn of 1993, the SWALES experiment provided the opportunity to compare the directional wave spectra derived from the Sonic Buoy/BMP combination with spectra from a nearby Datawell Directional Waverider Buoy (DWR). This opportunity was pursued in mid 1994 under funding from the NERC MASD Technology Fund.

This document describes briefly the BMP data acquisition process; it then details the processes involved in conversion of the raw BMP data to buoy motion and, finally, the derivation of directional wave spectra.

An analysis of the comparison between the DWR and BMP spectra is given. Appendices give a detailed description of the analysis techniques developed, concluding with illustrations of the complete set of comparison directional spectra obtained during SWALES.

KEYWORDS

ISSUING ORGANISATION

Institute of Oceanographic Sciences
Deacon Laboratory
Wormley, Godalming
Surrey GU8 5UB. UK.

Director: Colin Summerhayes DSc

Telephone Wormley (0428) 684141
Telex 858833 OCEANS G.
Facsimile (0428) 683066

Copies of this report are available from: ***The Library,*** *PRICE* *£0.00*

Index

1. Introduction

The purpose of the work reported upon was to develop and verify techniques for the derivation of Buoy Motion Data from data collected by a Buoy Motion Package (BMP) and for the subsequent derivation of Directional Wave Spectra.

The BMP was initially developed for use in the Sonic Buoy Hull Seakeeping Trials. These trials were carried out in April 1993 to test the improvements of hull and mooring configuration changes instigated following the capsize of the prototype buoy during its first deployment on the ERS1 CAL/VAL cruise.

The BMP was designed to provide a full description of the motion of the buoy, i.e. 3 components of displacement (Vertical, East-West and North-South) and 3 rotations (Yaw, Pitch and Roll). The displacements were to be valid over the gravity wave spectrum, i.e. from about 0.05 to 0.5 Hz. The rotations would ideally be valid over the range 0 to 0.5 Hz.

The BMP was required to be physically small and power consumption had to be kept to a minimum, so as not to result in an excessive reduction in the main buoy battery life.

So as to obtain a varied data set, sensor data were to be conditionally sampled, depending upon wind speed, and recorded within the package; a selected set of parameters were also to be output to an ARGOS transmitter for diagnostic purposes.

The size and power restrictions precluded the use of any form of stabilised platform, so that it was decided to use strapped-down 3-component accelerometers, rate gyroscopes and magnetometers in conjunction with 2 pendulous inclinometers. By suitable combination of the inclinometer data (valid for frequencies below the gravity wave spectrum) and the integrated x- and y-axis rate gyroscope data (valid over the gravity wave spectrum), it was anticipated that "pitch" and "roll" angles could be derived. These would then be used in conjunction with the magnetometer data to derive buoy heading (yaw angle) and buoy tilt angles in the East-West and North-South planes. The resulting buoy orientation would also be used to rotate the 3 acceleration components to Vertical, East-West and North-South components, which would be doubly integrated to equivalent displacements.

In the first instance, the above processing was to be carried out subsequent to the recovery of the buoy since insufficient time was available for development and testing of the conversion algorithms prior to the deployment. Additionally it was not known whether the processor would be fast enough to cope with real-time processing and it was, in any event, desirable to acquire some raw data for test purposes.

The BMP was also incorporated in the Sonic Buoy for the SWALES experiment, during which a Datawell Directional Waverider buoy (DWR) was continuously deployed near the Sonic Buoy to acquire directional wave data. This gave an opportunity to compare directional wave spectra, derived from the BMP data (and assuming that the Sonic Buoy acted as a good slope-follower), with directional wave spectra of proven quality. This report describes work carried out to derive the Sonic Buoy motion from the BMP data acquired during SWALES and compares the resulting derived directional wave spectra with those obtained from the DWR.

2. Raw Data Acquisition

The BMP used the following sensors:

3 orthogonally mounted accelerometers, type AMD-CK/0-A-2 (Scientific Electro Systems Ltd.) giving analogue outputs nominally of 1V/g with an offset of +2.5V (range ±2g, where g = 9.81 metres/sec^2)

3 orthogonally mounted solid state rate gyroscopes, type ENV-05S (Murata Electronics (UK) Ltd.), giving analogue outputs nominally of 22 mV/deg/sec with an offset of +2.5V (range ±90 deg/sec)

3 component magnetometer, type HR3MA (THORN EMI Electronics Ltd.), giving analogue outputs nominally of 66.7 mV/nT with no offset.

2 orthogonally mounted inclinometers, type 3920 (Penny & Giles Potentiometers Ltd.), having a range of ±178 degrees.

+ an external Young AQ anemometer for wind speed and direction to trigger the conditional sampling

The sensor outputs were conditioned by circuits giving a common output range of +2.5V ± 2V full scale; these were followed by anti-aliasing low pass filters with a cut-off frequency of 2 Hz.

The system used for acquiring the sensor data was a DSP Designs Ltd. GCAT3000, PC-XT compatible, single board computer, with a GCAT2000 peripherals card containing an 8 input 12 bit analogue to digital convertor. By connecting the 8th input to a +2.5V reference, this could handle 7 inputs with the above-defined range. It was necessary to incorporate an additional level of (external) analogue multiplexing to accommodate the number of analogue channels. This was achieved by using CMOS analogue gates on the low pass filter cards, with an 8 channel analogue bus, with control by the GCAT OP2 line. By the use of interrupt-driven routines in the software, it was possible to acquire 16 channels within a few mS at a sampling rate of 4 Hz. The interchannel sampling delay was considered to be small enough to make timing corrections unnecessary. The resulting 12 bit data were conditionally saved as 16 bit (2 byte) words to a 4 Mbyte, type 1, PCMCIA flash card in a format developed for this application.

Data "records" of 640 seconds length (2560 samples) were initiated whenever the following conditions were simultaneously met:

- system clock time was a multiple of 3 hours, e.g. 0000, 0300, 0600 . . . .
- number of previous records for the range in which the current (1 minute) mean wind speed lay was less then the predetermined limit, ranges and limits being as defined below:

Wind Speed Range (m/s)	0-5	5-10	10-15	15-20	20+
Maximum number of records	4	10	13	12	8

In addition, the BMP conditional sampling scheme included a function similar to the "blackbox" recorders used to record aircraft flight data prior to a crash. In the BMP, "blackbox" records of preceding 32 seconds of data were made whenever the pitch and/or roll angle, as indicated by the inclinometers, exceeded 175 degrees, i.e. a full capsize.

3. Recovery of Raw Data Files

The operations required to recover the BMP records are summarised in figure 1, below.

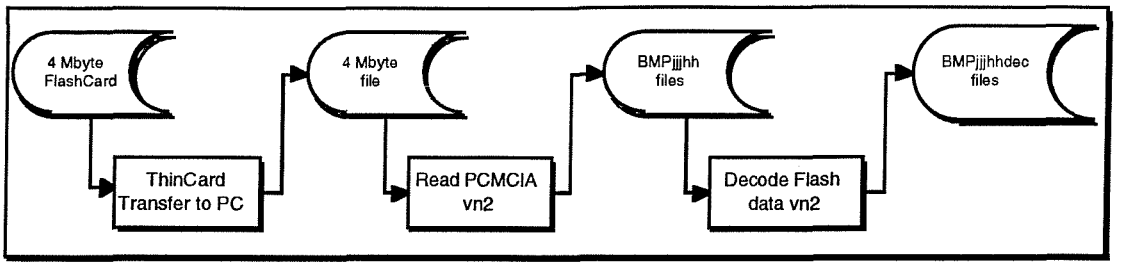

Figure 1 Recovery of Flash Card Data

After recovery of the buoy, the flashcard contents were transferred to individual 80 kbyte files on a Macintosh as described in Appendix C.3. The "blackbox" records made when the buoy capsized amounted to 2.1 Mbytes (the capacity remaining when the buoy overturned. This was because the buoy pitch and roll motion in the inverted state resulted in repeated triggering of the "blackbox" condition.

3.1 1st SWALES Deployment

The binary data files retrieved from the flashcard are given below:

Filename	Bin	BMP MWS m/s	Young MWS m/s	Sonic MWS m/s	Sonic Wind Dir'n from
BMP28615	1	0	0	0	n/a
BMP28618	1	0	0	0	n/a
BMP28621	1	0	0	0	n/a
BMP28700	1	0	0	0	n/a
BMP29315	2	7	8.2	7.9	73.1
BMP29318	2	9	9.2	9.1	60.3
BMP29321	2	10	9.7	9.4	137.8
BMP29400	2	8	9.4	8.7	9.9
BMP29403	2	7	7.7	7.3	10.8
BMP29406	2	9	8.9	8.7	n/a
BMP29409	2	7	7.4	7.2	n/a
BMP29412	2	7	8.5	8.2	41.0
BMP29415	2	10	10.6	10.3	36.3
BMP29418	2	8	9.1	8.7	34.6
BMP30612	3	11	11.8	11.5	148.5
BMP30615	3	11	12.6	12.2	154.2
BMP30618	3	11	12.1	11.6	149.0
BMP30621	3	12	12.1	11.7	147.1
BMP30700	3	12	12.5	12.3	150.8
BMP30703	3	11	11.2	10.6	153.1
BMP31309	3	11	12.2	11.8	325.0
BMP31312	3	12	13.7	13.1	329.5
BMP31314	BB	12	13.5	13.1	318.8

where the filename BMPjjjhh indicates the Julian Day (jjj) and the time (hh) in hours. BB indicates a "blackbox" record. Note that the BMP mean wind speed (MWS) is the 1 minute mean prior to initiation of the record, whereas the Sonic and Young values are 10 minute means, starting at the times shown. The records for days 286 and 287 were pre deployment.

The files for days 293 - 313 were converted to decimal form, using the QuickBasic application Decode Flash data vn2, resulting in ASCII files BMPjjjhhdec

3.2 2nd SWALES Deployment

The BMP clock appears to have been incorrectly initialised and, as a result, timings of records have to be inferred from the indicated timings relative to the known start up time. The BMP rebooted four times during the deployment (always during a record). The estimated accuracy of the inferred times of the records is ± 1 hour. The BMP 1 minute mean wind speeds are in reasonably good agreement with the Young and Sonic 10 minute means from the Formatter data (ref. 1).

The binary data files retrieved from the flashcard are given below:

Filename	Bin	BMP MWS m/s	Young MWS m/s	Sonic MWS m/s	Sonic Wind Dir'n from
BMP32512	1	0	0	0	n/a
BMP32515	1	0	0	0	n/a
BMP32518	1	0	0	0	n/a
BMP32521	1	0	0	0	n/a
BMP32709	2	6	6.7	6.5	188.0
BMP32715	2	6	6.8	6.4	182.5
BMP32718	2	7	8.7	8.3	176.5
BMP32721	2	8	8.7	8.3	243.3
BMP32800	2	8	9.6	9.3	239.8
BMP32803	"5"	"3"	11.5	11.2	212.6
BMP32806	3	12	12.9	12.7	188.4
BMP32809	3	12	12.5	12.1	194.7
BMP32812	3	13	14.0	13.5	235.3
BMP32815	2	9	10.8	10.5	217.3
BMP32818	3	10	11.8	11.5	21.1
BMP32821	2	9	11.4	10.9	18.4
BMP32900	2	7	9.6	9.2	13.5
BMP33121	3	14	14.1	13.8	154.8
BMP33206	3	13	14.5	14.3	165.5
BMP33209	3	14	13.5	13.1	161.6
BMP33212	3	13	15.6	15.3	171.2
BMP33215	3	12	13.3	13.0	207.4
BMP33218	3	14	15.4	14.7	172.6
BMP33221	3	14	14.5	14.1	181.1
BMP33300	3	12	13.4	13.1	181.9

4. Conversion of Raw BMP Data to Buoy Motion

The conversion of the (decimal) raw BMP data to useful time series, which was carried out by the QuickBasic application Calibrate vn7, is summarised in figure 2, below.

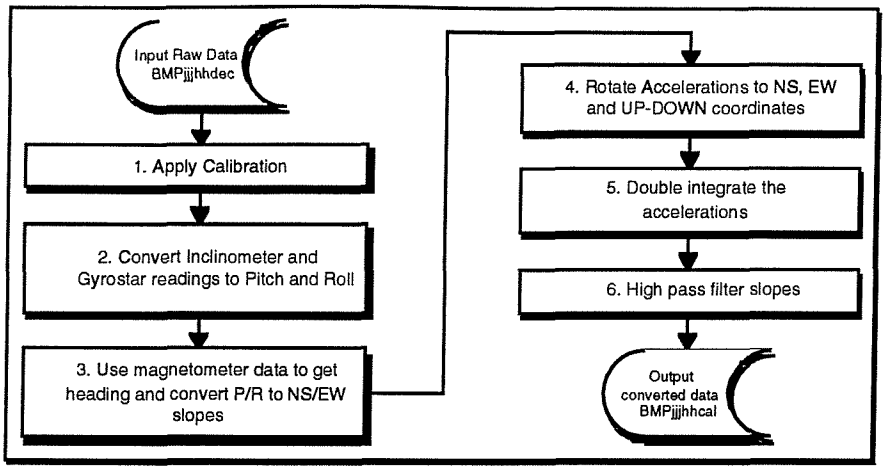

Figure 2 Conversion of Raw Data to Displacements and Slopes

4.1 Application of Calibrations

The BMP was calibrated before and after the deployment using a special version of the acquisition application named GCMAIN3.T This application, which was blown into an alternative calibration GCAT EPROM (together with appropriate DOS system files, drivers, etc.) allows one to examine the raw data in the acquisition buffer using a VDU connected to the BMP's GCAT video output connector.

The accelerometers were calibrated using the Earth's gravitational acceleration (9.81 m/s^2) by orienting the respective sensor axis up, down or horizontal.

The rate gyroscopes were calibrated using an oscillatory test rig developed by the Acoustics Team for the Gyrostar calibration.

Because of lack of time, the magnetometers were only given an approximate calibration in the lab, orienting the sensor axes at various angle to the Earth's field. After the deployments, repeat calibrations obtained in this manner were not satisfactory, indicating possible damage to the sensor at some stage of the experiments, possibly due to excessive shocks when the buoy was driven onto the rocks in the river Tywi estuary.

The inclinometers were tested by tilting the BMP to various angles measured with a spirit level gauge.

Calibration coefficients used in processing the data were as listed in the following table, where engineering units are given by a*(digital units + b)

Note that "N" refers to the BMP housing North reference mark, positive Yaw represents clockwise rotation looking down on the buoy from above. Inclinometer "NS" and "EW" are +ve for buoy North and East down, respectively. Angular Rate "NS" and "EW" are +ve for buoy North and East moving down, respectively. Note that the calibrations of the Magnetic Field channels in terms of absolute engineering units are unimportant and that, in the absence of more reliable information, their calibration coefficients have been set to 1. This does not, of course, correct for magnetic deviations.

Signal (mnemonic)	a	b
Acceleration "N" (a_n)	-6.0037e-3	56
Acceleration "E" (a_e)	5.9491e-3	48
Acceleration "UP" (a_u)	5.9383e-3	18
Inclinometer "NS" (I_{ns})	7.6382e-4	21
Inclinometer "EW" (I_{ew})	7.9014e-4	-76
Angular Rate "NS" (G_{ns})	4.5624e-4	-79
Angular Rate "EW" (G_{ew})	4.5584e-4	6
Angular Rate Yaw (G_{ud})	-4.6332e-4	-98
Magnetic Field "N" (H_n)	1	0
Magnetic Field "E" (H_e)	1	0
Magnetic Field "UP" (H_u)	1	0

4.2 Conversion of Inclinometer and Rate Gyroscope data to Pitch and Roll

As stated in 1, above, the inclinometer signals should be valid for frequencies below the gravity wave spectrum, i.e. where there are negligible horizontal accelerations acting upon the pendulous sensors. The rate gyroscope data, when integrated, give valid angular variations over the gravity wave spectrum. At very low frequencies, well below the gravity wave spectrum, rate gyroscope sensor noise (when integrated) is excessive.

Consequently, the approach in the digital signal processing was to add the low pass filtered inclinometer signals to the high pass filtered integrated rate gyroscope signals; this is illustrated by the schematic diagram given in Figure 3, below.

The filter transfer functions shown in Figure 3 use the following component functions, where s is the complex frequency:

$$G1(s) = \frac{-\beta.\omega_1^2}{s^2 + \alpha.\omega_1.s + \beta.\omega_1^2}$$ i.e. low pass filter, cut-off frequency ω_1

$$G2(s) = \frac{1}{s + \omega_2}$$ i.e. "leaky" integrator, cut-off frequency ω_2

The output from the summer is $\theta(s)$. These transfer functions were used in preference to more ideal filters as they are physically realisable in an analogue processing circuit, should that approach prove more attractive for a real-time conversion system.

After some experimentation, the cut-off frequencies ω_1 and ω_2 were chosen to be $2\pi/40$ radians/second and a Bessel Response was used ($\alpha = 2.2032027$, $\beta = 1.618034$).

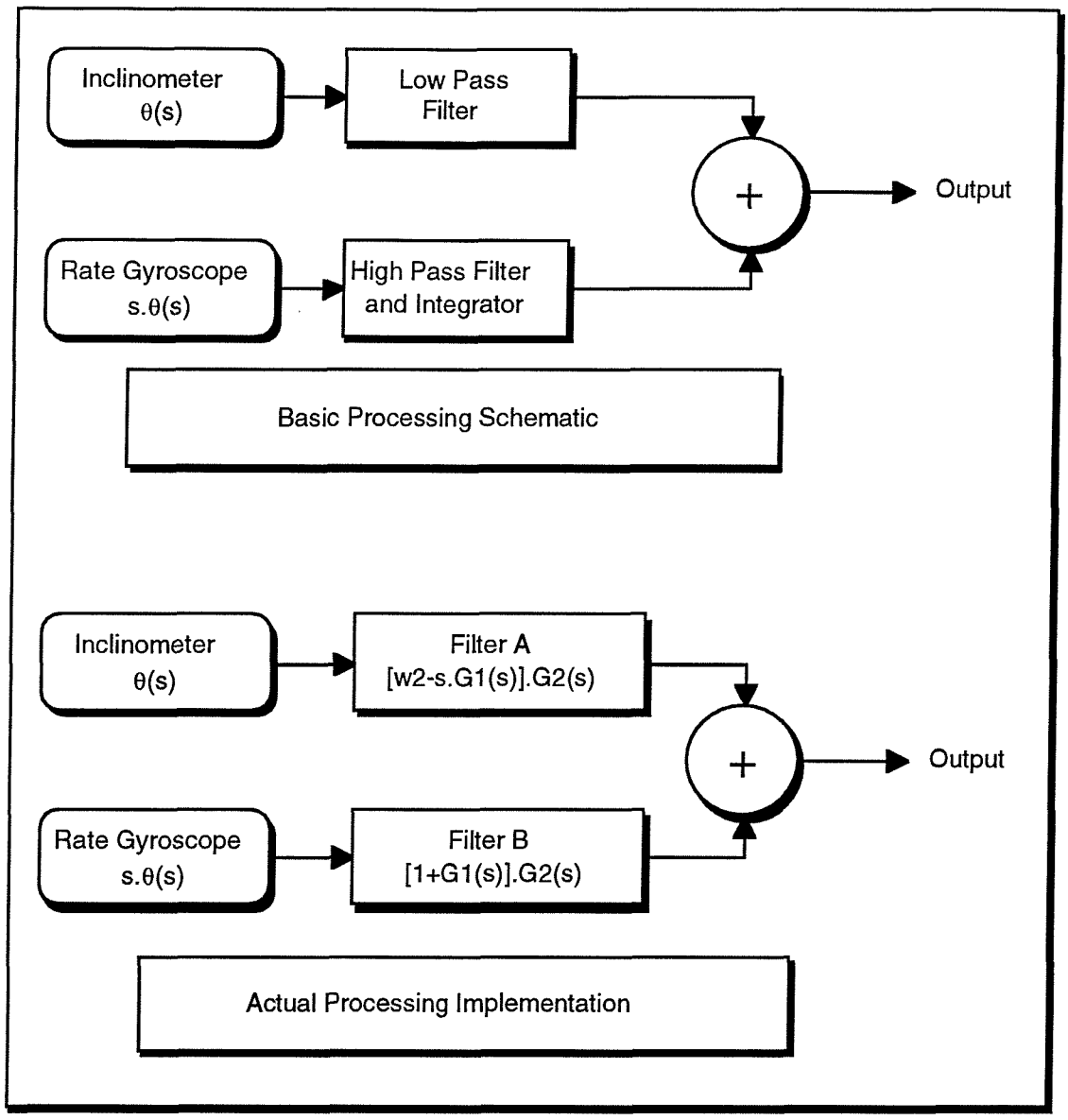

Figure 3. Conversion of Inclinometer and Rate Gyro Data to Pitch and Roll

The magnitude and phase responses of the two filters are shown in Figures 4 and 5, below. It will be seen that, in order to achieve an overall unity gain, zero phase θ(s) output from the summer, the individual filters have slight peaks. These result in fairly well damped transient oscillations for a step input so that, when processing a finite record, it is necessary to let the filter outputs settle. The digital double integrators/filters used to derive the displacement signals from the acceleration signals similarly exhibit transient responses. For this reason, the first 400 samples (100 seconds) are not used in subsequent analysis.

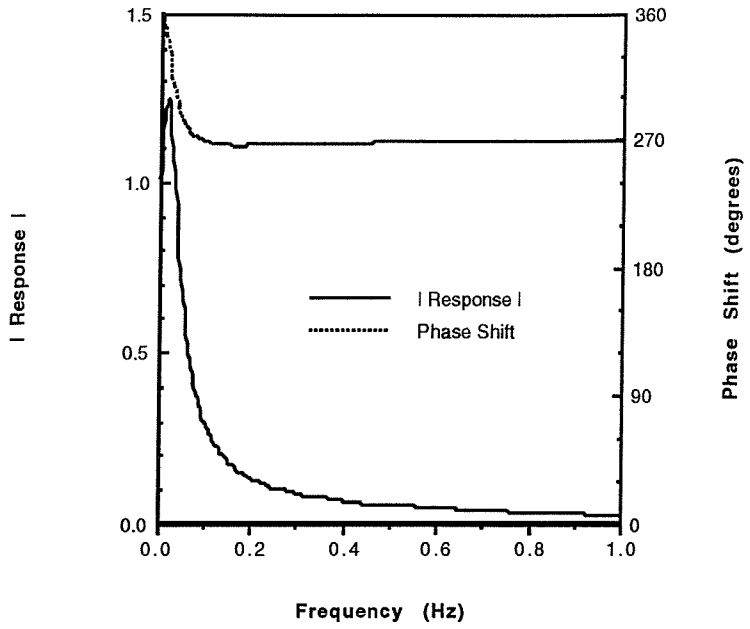

Figure 4. Filter A Response, $[\omega_2 - s.G1(s)].G2(s)]$, $s = j.2\pi.Frequency$

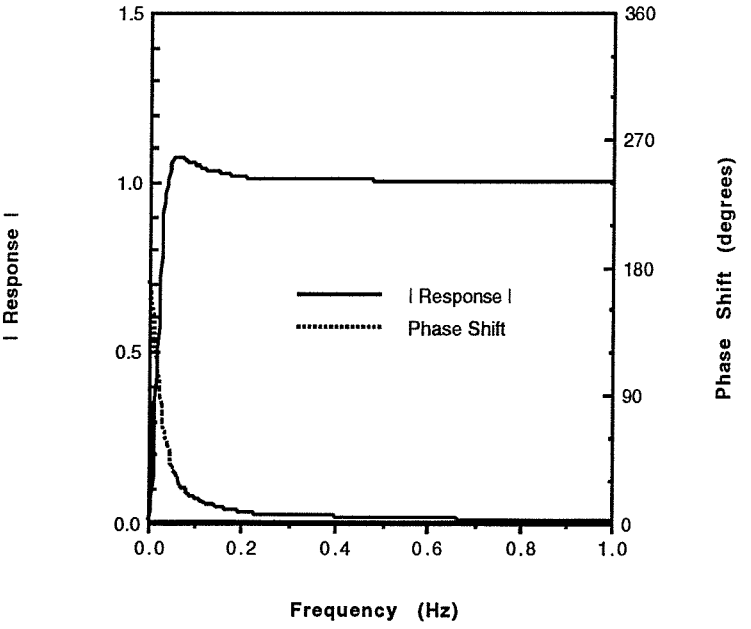

Figure 5. Filter B response relative to perfect integrator, $s.G2(s).[1 + G1(s)]$,

$s = j.2\pi.Frequency$

The infinite impulse response system functions equivalent to the two filter responses were calculated, using the bilinear transformation (Appendix A), to be of the form:

$$H(z) = \frac{b_0 + b_1.z^{-1}\ b_2.z^{-2} + b_3.z^{-3}}{1 - a_1.z^{-1} - a_2.z^{-2} - a_3.z^{-3}}$$

For filter A:

$$b_0 = \frac{\omega_2.[\omega_2.T + (\beta.\omega_1^2 + \alpha.\omega_1.\omega_2).T^2 + \beta.\omega_1^2.\omega_2.T^3]}{D}$$

$$b_1 = \frac{\omega_2.[-\omega_2.T + (\beta.\omega_1^2 + \alpha.\omega_1.\omega_2).T^2 + 3.\beta.\omega_1^2.\omega_2.T^3]}{D}$$

$$b_2 = \frac{\omega_2.[-\omega_2.T - (\beta.\omega_1^2 + \alpha.\omega_1.\omega_2).T^2 + 3.\beta.\omega_1^2.\omega_2.T^3]}{D}$$

$$b_3 = \frac{\omega_2.[\omega_2.T - (\beta.\omega_1^2 + \alpha.\omega_1.\omega_2).T^2 + \beta.\omega_1^2.\omega_2.T^3]}{D}$$

$$a_1 = \frac{3 + \omega_2 T + \alpha.\omega_1.T - \alpha.\omega_1.\omega_2.T^2 - \beta.\omega_1^2.T^2 - 3.\beta.\omega_1^2.\omega_2.T^3}{D}$$

$$a_2 = \frac{-3 + \omega_2 T + \alpha.\omega_1.T + \alpha.\omega_1.\omega_2.T^2 + \beta.\omega_1^2.T^2 - 3.\beta.\omega_1^2.\omega_2.T^3}{D}$$

$$a_3 = \frac{1 - \omega_2 T - \alpha.\omega_1.T + \alpha.\omega_1.\omega_2.T^2 + \beta.\omega_1^2.T^2 - \beta.\omega_1^2.\omega_2.T^3}{D}$$

where

T is half the sampling interval, i.e. 0.125 second, and

$$D = 1 + \omega_2.T + \alpha.\omega_1.T + \alpha.\omega_1.\omega_2.T^2 + \beta.\omega_1^2.T^2 + \beta.\omega_1^2.\omega_2.T^3$$

For filter B:

$$b_0 = \frac{\omega_2.T.[1 + \alpha.\omega_1.T]}{D}$$

$$b_1 = \frac{\omega_2.T.[-1 + \alpha.\omega_1.T]}{D}$$

$$b_2 = -b_0$$

$$b_3 = -b_1$$

$$a_1 = \frac{3 + \omega_2 T + \alpha.\omega_1.T - \alpha.\omega_1.\omega_2.T^2 - \beta.\omega_1^2.T^2 - 3.\beta.\omega_1^2.\omega_2.T^3}{D}$$

$$a_2 = \frac{-3 + \omega_2 T + \alpha.\omega_1.T + \alpha.\omega_1.\omega_2.T^2 + \beta.\omega_1^2.T^2 - 3.\beta.\omega_1^2.\omega_2.T^3}{D}$$

$$a_3 = \frac{1 - \omega_2 T - \alpha.\omega_1.T + \alpha.\omega_1.\omega_2.T^2 + \beta.\omega_1^2.T^2 - \beta.\omega_1^2.\omega_2.T^3}{D}$$

For the k^{th} sample, the output, y, is given in terms of the input, x, by:

$$y[k] = a_1.y[k-1] + a_2.y[k-2] + a_3.y[k-3]$$
$$+ b_0.x[k] + b_1.x[k-1] + b_2.x[k-2] + b_3.x[k-3]$$

The above processing is carried out on the two pairs of signals, the filter outputs being simply summed, i.e.

Inclinometer "NS" (filtered by Filter A) with Rate Gyroscope "NS" (filtered by Filter B), giving Pitch, p

and

Inclinometer "EW" (filtered by Filter A) with Rate Gyroscope "EW" (filtered by Filter B),, giving Roll, r

4.3 Use of magnetometer data to convert p/r to NS/EW slopes

The three magnetometer components are now used to compute the buoy heading and to translate the pitch and roll derived in 4.2, above, to NS and EW slopes.

The algorithms required to do this are as follows (ref. 2):

$H_v = \sin(P).H_n + \sin(r).H_e - H_u.\sqrt{1 - \sin^2(p) - \sin^2(r)}$ Vertical Component of field

$H_h = \sqrt{H_n^2 + H_e^2 + H_u^2 - H_v^2}$ Horizontal Component of field

The buoy magnetic heading, ψ, is given by:

$$\sin(\psi) = \frac{H_n + \sin(r).H_u - \sin(r).\left(\frac{\sin(p).H_n + \sin(r).H_e}{1 + \sqrt{1 - \sin^2(p) - \sin^2(r)}}\right)}{H_h}$$

$$\cos(\psi) = \frac{H_n + \sin(P).H_u - \sin(p).\left(\frac{\sin(p).H_n + \sin(r).H_e}{1 + \sqrt{1 - \sin^2(p) - \sin^2(r)}}\right)}{H_h}$$

and the buoy tilt angles are given by:

$$\text{NS slope} = -\frac{\sin(p).\cos(\psi) + \sin(r).\sin(\psi)}{\sqrt{1 - \sin^2(p) - \sin^2(r)}}$$ +ve for N down

$$\text{EW slope} = -\frac{\sin(p).\sin(\psi) - \sin(r).\cos(\psi)}{\sqrt{1 - \sin^2(p) - \sin^2(r)}}$$ +ve for E down

4.4 Rotation of Accelerations to NS, EW and UP-DOWN co-ordinates

The calculated pitch and roll angles are now used to translate the three acceleration components to orthogonal N', E' and U' components (NB not magnetic NS and EW, although true Vertical). The orientations are shown in Figure 6, overleaf.

The cosine of the angle between the axis of rotation and the S axis is given by:

$$\alpha = \frac{\sin(r)}{\sqrt{\sin^2(r) + \sin^2(p)}} \cdot \frac{1}{\sqrt{1 - \sin^2(p)}}$$

The cosine of the angle between the axis of rotation and the E axis is given by:

$$\beta = \frac{\sin(p)}{\sqrt{\sin^2(r) + \sin^2(p)}} \cdot \frac{1}{\sqrt{1 - \sin^2(r)}}$$

The cosine of the angle between the axis of rotation and the U (true vertical) axis is given by:

$\gamma = \cos(\pi/2) = 0$

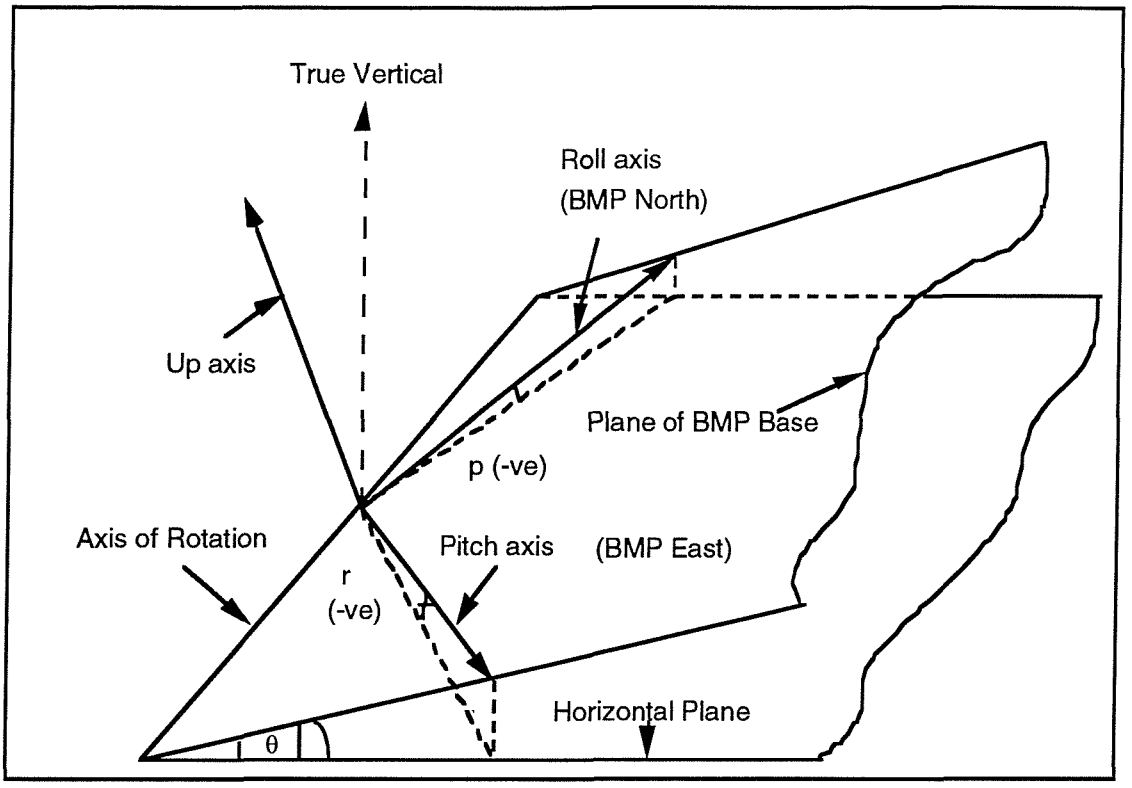

Figure 6. BMP axes

The angle of rotation, θ, about the axis of rotation is given by:

$$\sin(\theta) = -\sqrt{\sin^2(r) + \sin^2(p)}$$

$$\cos(\theta) = \sqrt{1 - \sin^2(r) - \sin^2(p)}$$

and the rotation matrix is then given by:

$$\begin{vmatrix} \cos(\theta) + \alpha^2.(1 - \cos(\theta)) & \gamma.\sin(\theta) + \alpha.\beta.(1 - \cos(\theta)) & -\beta.\sin(\theta) + \alpha.\gamma.(1 - \cos(\theta)) \\ -\gamma.\sin(\theta) + \beta.\alpha.(1 - \cos(\theta)) & \cos(\theta) + \beta^2.(1 - \cos(\theta)) & \alpha.\sin(\theta) + \beta.\gamma.(1 - \cos(\theta)) \\ \beta.\sin(\theta) + \gamma.\alpha.(1 - \cos(\theta)) & -\alpha.\sin(\theta) + \gamma.\beta.(1 - \cos(\theta)) & \cos(\theta) + \gamma^2.(1 - \cos(\theta)) \end{vmatrix}$$

So that the rotated accelerations are given by:

$$\begin{vmatrix} a_n' \\ a_e' \\ a_u' \end{vmatrix} = \begin{vmatrix} a_n \\ a_e \\ a_u \end{vmatrix} . \begin{vmatrix} \cos(\theta) + \alpha^2.(1 - \cos(\theta)) & \gamma.\sin(\theta) + \alpha.\beta.(1-\cos(\theta)) & -\beta.\sin(\theta)+\alpha.\gamma.(1-\cos(\theta)) \\ -\gamma.\sin(\theta)+\beta.\alpha.(1-\cos(\theta)) & \cos(\theta) + \beta^2.(1 - \cos(\theta)) & \alpha.\sin(\theta) + \beta.\gamma.(1-\cos(\theta)) \\ \beta.\sin(\theta)+\gamma.\alpha.(1 - \cos(\theta)) & -\alpha.\sin(\theta)+\gamma.\beta.(1-\cos(\theta)) & \cos(\theta) + \gamma^2.(1 - \cos(\theta)) \end{vmatrix}$$

4.5 Double integration of the accelerations

The three rotated acceleration components were then digitally double integrated to displacements, using a 4th order Bessel band pass filter in each case; such a filter is equivalent to a perfect double integrator combined with a 4th order Bessel high pass filter.

The combined integrator/filter response used was:

$$H(s) = \left(\frac{1}{s^2}\right).\left(\frac{s^4}{s^4 + \alpha_1.\omega_o.s^3 + \alpha_2.\omega_o{}^2.s^2 + \alpha_3.\omega_o{}^3.s + \alpha_4.\omega_o{}^4}\right)$$

where

$\omega_o = 2\pi/40$ radians/second

$\alpha_1 = 4.6945932$

$\alpha_2 = 9.9176425$

$\alpha_3 = 10.863836$

$\alpha_4 = 5.1001291$

The infinite impulse response system function equivalent of this response was calculated by the bilinear transformation to be:

$$H(z) = \frac{b_0 + b_1.z^{-1} + b_2.z^{-2} + b_3.z^{-3} + b_4.z^{-4}}{1 - a_1.z^{-1} - a_2.z^{-2} - a_3.z^{-3} - a_4.z^{-4}}$$

where

$b_0 = .014255286$

$a_1 = 3.81739566$ $\quad b_1 = 0$

$a_2 = -5.46705723$ $\quad b_2 = -0.028510572$

$a_3 = 3.48130528$ $\quad b_3 = 0$

$a_4 = -.831654707$ $\quad b_4 = .014255286$

so that, for the k^{th} sample, the output, y, is given in terms of the input, x, by:

$$y[k] = a_1.y[k-1] + a_2.y[k-2] + a_3.y[k-3] + a_4.y[k-4]$$
$$+ b_0.x[k] + b_1.x[k-1] + b_2.x[k-2] + b_3.x[k-3] + b_4.x[k-4]$$

The N' and E' components can then be rotated to magnetic NS and EW, if required; this was not done as the subsequent directional analysis used only the vertical displacement and the NS and EW slopes.

4.6 High pass filtering of slopes

In order to maintain comparability between the spectra of vertical displacement and slope energy, it was necessary to apply similar high pass filters as used in the double integration processing to the slope signals, i.e. a 4th order Bessel high pass filter with the response:

$$H(s) = \frac{s^4}{s^4 + \alpha_1.\omega_o.s^3 + \alpha_2.\omega_o{}^2.s^2 + \alpha_3.\omega_o{}^3.s + \alpha_4.\omega_o{}^4}$$

where

$\omega_o = 2\pi/40$ radians/second

$\alpha_1 = 4.6945932$

$\alpha_2 = 9.9176425$

$\alpha_3 = 10.863836$

$\alpha_4 = 5.1001291$

The infinite impulse response system function equivalent of this response was calculated by the bilinear transformation to be:

$$H(z) = \frac{b_0 + b_1.z^{-1} + b_2.z^{-2} + b_3.z^{-3} + b_4.z^{-4}}{1 - a_1.z^{-1} - a_2.z^{-2} - a_3.z^{-3} - a_4.z^{-4}}$$

where

$b_0 = 0.9123383$

$a_1 = 3.81739566$ $b_1 = -3.6493532$

$a_2 = -5.46705723$ $b_2 = 5.4740298$

$a_3 = 3.48130528$ $b_3 = -3.6493532$

$a_4 = -.831654707$ $b_4 = 0.9123383$

so that, for the k^{th} sample, the output, y, is given in terms of the input, x, by:

$$y[k] = a_1.y[k-1] + a_2.y[k-2] + a_3.y[k-3] + a_4.y[k-4]$$
$$+ b_0.x[k] + b_1.x[k-1] + b_2.x[k-2] + b_3.x[k-3] + b_4.x[k-4]$$

The above processing was carried out on the BMPjjjhhdec files, and the three components of displacement and the two slopes were saved to BMPjjjhhcal files.

5. Derivation of Directional Wave Spectrum

The Vertical Displacement, NS slope and EW slope data from the BMPjjjhhcal files were first spectrally analysed, using the QuickBasic application Spectrum. The processing is shown in figure 7, below.

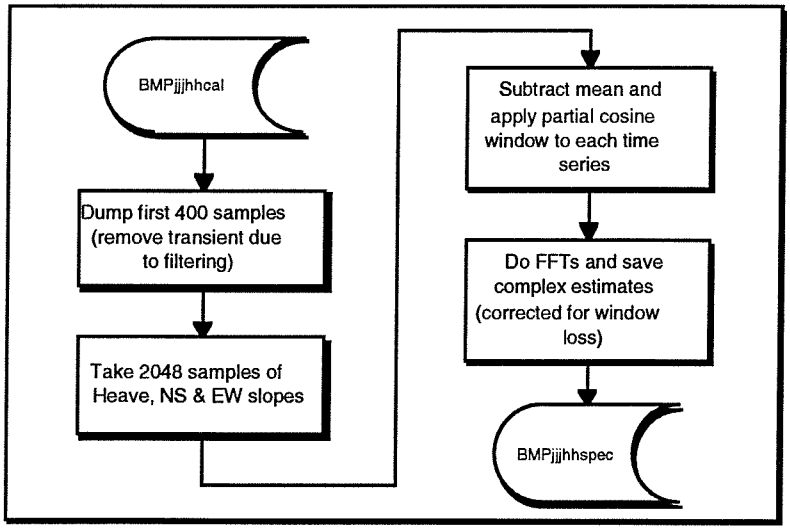

Figure 7. Spectral Analysis of Heave and Slopes

A simple QuickBasic application, specrms1, as described in Appendix C.5, was then used to derive the values of Hs and Tz from the heave spectrum, to plot the heave and slope spectra and check ratio, and to save the spectrum in a file BMPjjjhhspec1 in a format suitable for entry into CricketGraph.

The resulting comparisons of Hs and Tz with the directional waverider (DWR) data are shown in figures 8 and 9, below. DWR values for the preceding and following half hours are included to give a measure of wave stationarity.

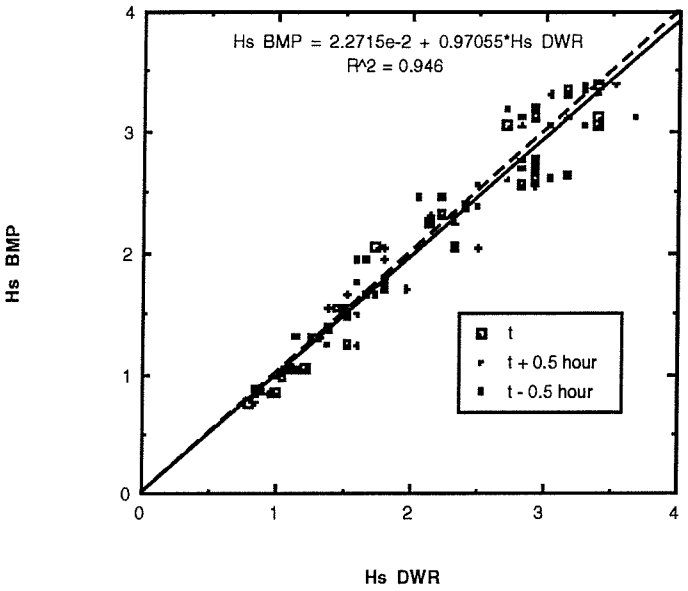

Figure 8. Comparison of BMP and DWR Hs values for nominal time and for ± 0.5 hour

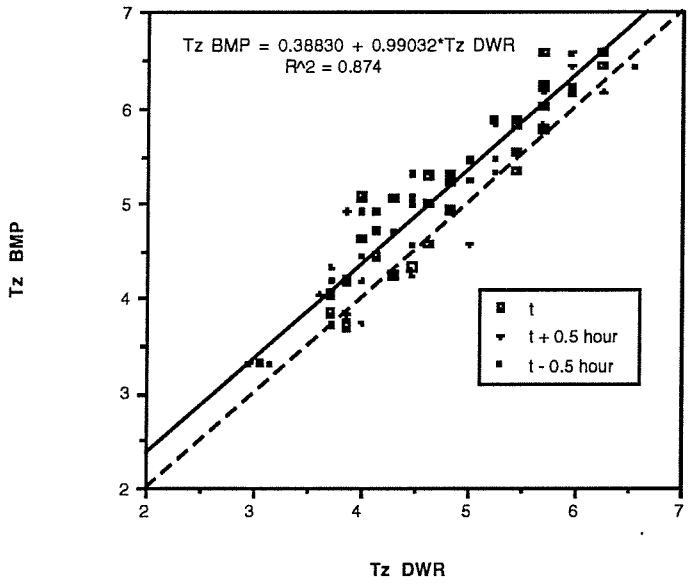

Figure 9. Comparison of BMP and DWR Tz values for nominal time and for ± 0.5 hour

The DWR values were obtained by analysis of 26.67 minutes of data, using spectral analysis of 2048 samples (at 1.28 Hz) in 8 x 256 sample sections, whereas the BMP values were obtained from 8.53 minutes of data, using spectral analysis of a single 2048 sample (at 4 Hz) section; so that the confidence limits for Hs, Tz and for estimates of a given spectral bandwidth are correspondingly narrower for the DWR estimates. A DWR spectral estimate of 0.005 Hz width,

has a chi-squared probability distribution with 16 degrees of freedom, giving a coefficient of variation of 35%, whereas the BMP spectral estimates have a width of 0.00195 Hz, so that the nearest equivalent to the DWR width, obtained by averaging 2 BMP estimates, has 4 degrees of freedom and a coefficient of variation of 71%.

A further QuickBasic application, Direction1, was then used to compute the directional wave spectrum, using the standard technique as summarised in Appendix C.5. This version of the application Direction converted the estimates to banded spectra with the same frequency bands as the equivalent DWR spectra. An example of the spectra produced, together with the matching DWR spectra, is given in figures 10-12, below.

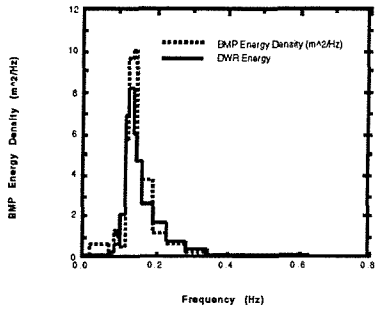

Figure 10. Comparison of BMP and DWR Energy spectra

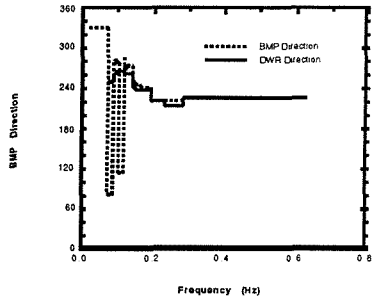

Figure 11. Comparison of BMP and DWR Mean Directions

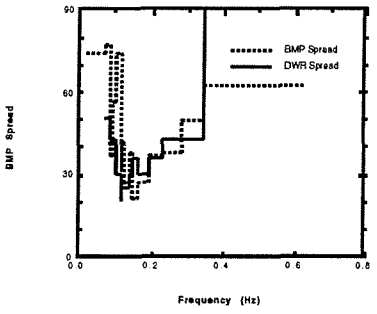

Figure 12. Comparison of BMP and DWR Mean Directional Spreads

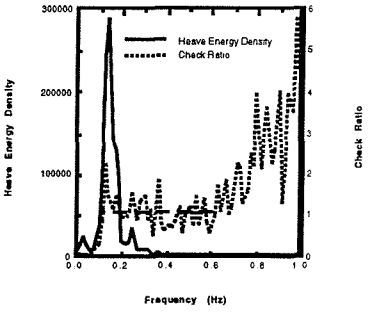

Figure 13. Energy Spectrum and Check Ratio for BMP31312

The agreement between the spectra is generally good, apart from the low frequency "noise" in the BMP direction spectrum. This is partially due to the banded presentation, which results in little smoothing of the BMP estimates for some bins. It must be reiterated that the BMP record is considerably shorter than that for the DWR and that, consequently, the BMP estimates have significantly higher uncertainties than the DWR at low frequencies.

The post-deployment magnetometer calibrations differed significantly from the pre-deployment calibrations, suggesting a sensor malfunction, as noted above. It is unlikely that the correct calibration can be recovered at this stage.

The average value of the Check Ratio (the ratio of the heave energy to the equivalent energy derived from the slope energy) between 0.1 and 0.6 Hz is 1.08; this is shown in figure 13, above. The ratio rises rapidly above this range, possibly due to mooring effects and the differing heave and pitch resonances of the buoy. Below 0.1 Hz, the computed slope energy

appears to be excessive, presumably due to noise in the BMP sensors. The dispersion relationship for shallow water depth was used in calculating the equivalent energy from the slope energy, as described in Appendix C.8, i.e.

$$\omega^2 = gk.\tanh(kh)$$

where h is the water depth (50 metres for the SWALES area)

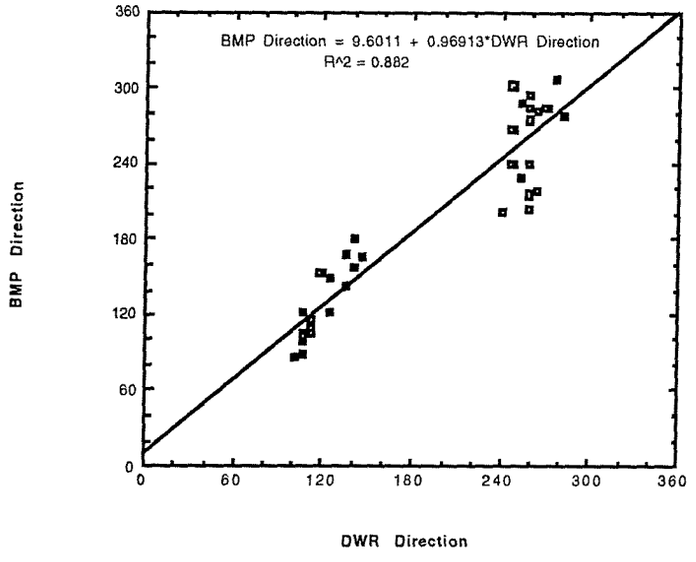

Figure 14. BMP Mean Direction vs DWR Mean Direction at peak of Energy Spectrum

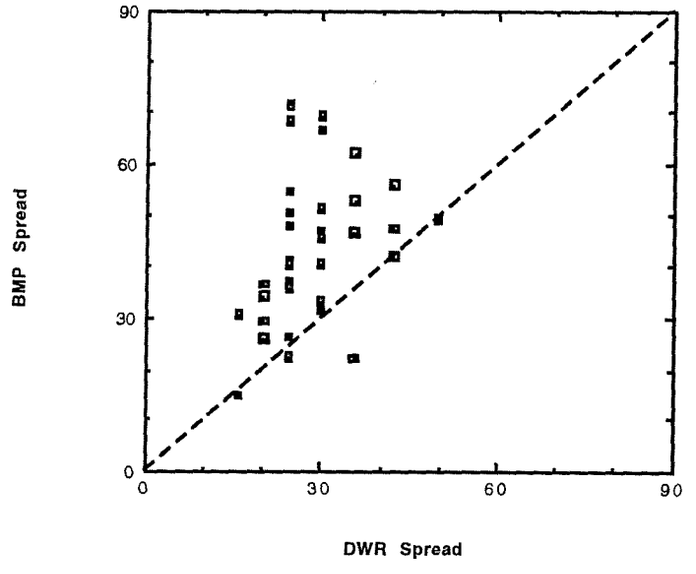

Figure 15. BMP Directional Spread vs DWR Directional Spread at peak of Energy Spectrum

The directional results from all the BMP records are illustrated by figures 14 and 15, above, which show the mean direction and directional spread at the peak of the spectrum for the BMP vs the DWR. There was no significant correlation of the ratio of BMP spread to DWR spread

with Hs or Tz, but this ratio was marginally greater for waves coming from the West., as shown in figure 16, below.

Many of the direction spectra with Westerly waves at the peak of the spectrum, were strongly bimodal, which may contribute to the scatter. Another possible cause is magnetic deviation due to the buoy components; unfortunately time and practicalities did not allow a proper "swing" of the buoy before deployment.

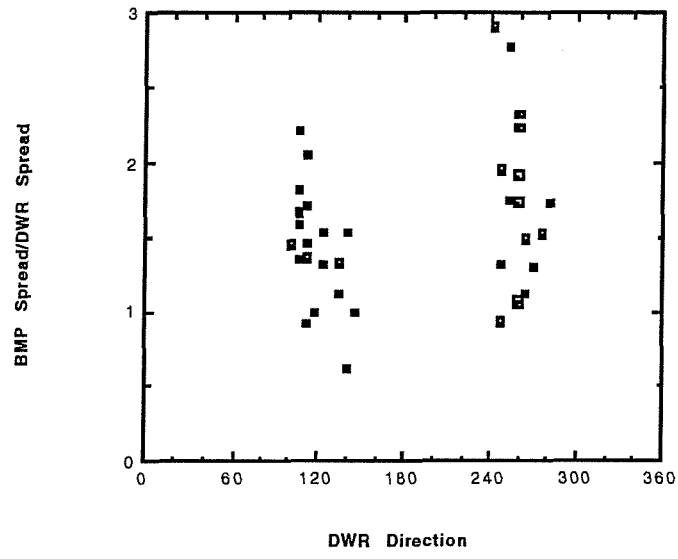

Figure 16. The ratio of the BMP spread to the DWR spread vs DWR peak direction

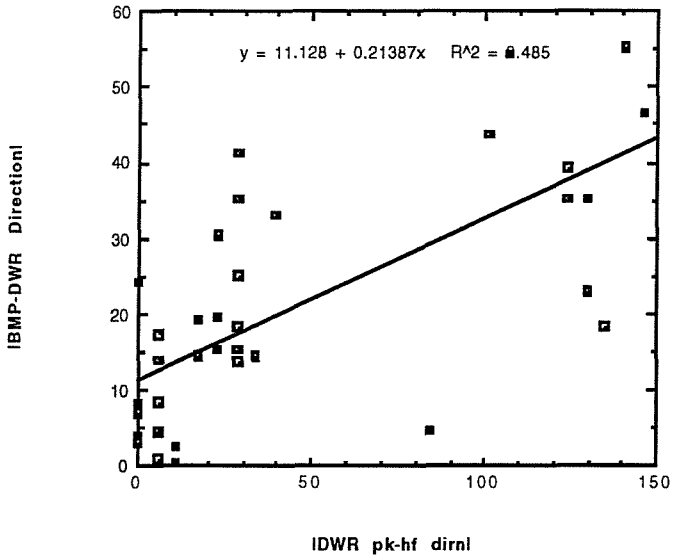

Figure 17. The modulus of the difference in the BMP/DWR peak directions vs the "directional width of the spectrum"

The difference in the peak directions measured with the two buoys shows some correlation with the "directional width of the spectrum", as expressed by the modulus of the difference in

the DWR directions at the peak of the energy spectrum and at 0.4 Hz; this is shown in figure 17, above.

6. Discussion

6.1 Introduction

The primary justification for developing the BMP was to investigate the Sonic Buoy seakeeping performance, following its capsize in the prototype form on RRS Charles Darwin cruise 62A. Ideally, the buoy should behave as a good surface slope follower, although the modelling studies and the moorings consequently used have been aimed more at ensuring the survivability of the buoy than at optimising the slope following performance.

Consequently, in carrying out a comparison of processed data with the DWR directional spectra, we are comparing the combined performance of two relatively untried systems (the dynamics of the Sonic Buoy and the sensing performance of the BMP) against a well tested system (the DWR). Ideally, further testing of the BMP and the validity of the associated processing should be made on a (preferably non-magnetic) motion testing rig; this could be pursued if further funding and manpower can be found and a suitable rig identified.

The algorithms for conversion of the BMP raw data to package motions are described above and in the Appendices. These algorithms have been developed specifically to provide an adequate description of motion over the spectral region of significant gravity wave motions.

The comparisons of BMP derived directional wave data with the DWR data are summarised in the following sections.

6.2 Hs and Tz parameters, Heave Spectra

- agreement is quite good, linear regression fits to the Hs and Tz plots being:

$$\text{Hs BMP} = 2.2715\text{e-}2 + 0.97055 * \text{Hs DWR} \qquad \text{with } R^2 = 0.946$$

$$\text{Tz BMP} = 0.38830 + 0.99032 * \text{Tz DWR} \qquad \text{with } R^2 = 0.874$$

Heave spectra are, given the shorter BMP record length (8.53 minutes actually analysed as opposed to 26.67 minutes for the DWR) , and hence wider confidence limits, remarkably similar (see figures E.1a-E.37a in Appendix E).

6.3 Mean Direction Spectra

- some comparisons with the DWR are not very satisfactory (see figures E.1b-E.37b in Appendix E); this is partly due to the differences in sampling and processing, but also possibly due to the BMP buoy/mooring performance in crossed seas. Best results were generally obtained in unimodal high wind/long wave conditions.

6.4 Spread Spectra

- these are encouraging, in that the spread is generally minimum at the peak of the energy spectrum (see figures E.1c-E.37c in Appendix E), but the values are usually significantly higher than for the DWR; this is normally a symptom of noise in the slope signals. Again, best results were obtained in unimodal high wind/long wave conditions.

6.5 Check Ratio

The Check Ratio (the ratio of the heave energy to the equivalent energy derived from the slope energy) is, on average, satisfactorily close to unity over the spectrum between 0.1 and 0.6 Hz, rising rapidly outside this range.

The combination of high spread and reasonable check ratio suggests that the Sonic Buoy's slope following response is satisfactory, but that there are errors in the derived NS and EW slopes, possibly due to the magnetic deviation

6.6 Overall assessment

In view of the complication, stated in 6.1, above, that the comparison is between a combination of two untried systems and a well tried system, the results are promising. The results show that the Sonic Buoy/BMP combination can give good one-dimensional wave data; there are also sufficient grounds for believing that good directional data can be achieved, given correct calibration of the magnetometer sensor. More experimental work on the actual hardware and on calibration and testing would be needed to take this any further.

7. Acknowledgements

This analysis was supported by the James Rennell Centre under the MASD Technology Fund arrangement; the author wishes to thank Dr. P.K.Taylor for his useful suggestions at the draft stage of this report. The author also wishes to acknowledge the considerable assistance provided by the Centre for Ocean Technology members of the Meteorological Team and by the IOSDL Moorings Team in obtaining the SWALES BMP and DWR data sets; without these data, this report would not have been possible.

8. References

1. Clayson, C.H. 1994, SWALES Sonic Buoy - Meteorological Data Report, IOSDL Internal Document, 40 pp.

2. Datawell bv "Preliminary Manual for the WAVEC buoy, Datawell bv, Laboratorium voor Instrumentatie, Haarlem, Netherlands, 38 pp.

3. Ewing, J.A. "Presentation and Interpretation of Directional Wave Data", Underwater Technology, vol. 12, no. 3, pp. 17-23

Appendix A Derivation of System Function from Transfer Function

Given a transfer function H(s) in terms of the complex frequency, s, one can calculate the system function, in terms of z, by making the substitution:

$$s = \left(\frac{2}{T}\right) \cdot \left(\frac{1 - z^{-1}}{1 + z^{-1}}\right)$$

where T is the sampling period.

The resulting H(z) can be simplified to the ratio of two polynomials in z^{-1}, e.g.

$$H(z) = \frac{\sum_{k=0}^{M} b_k.z^{-k}}{1 - \sum_{k=1}^{N} a_k.z^{-k}}$$

For example, if we have

$$H(s) = \frac{a}{s + a}$$

$$H(z) = \frac{a}{\left(\frac{2}{T}\right) \cdot \left(\frac{1 - z^{-1}}{1 + z^{-1}}\right) + a})$$

$$= T.a \cdot \left(\frac{1 + z^{-1}}{2.(1 - z^{-1}) + T.a.(1 + z^{-1})}\right)$$

$$= A \cdot \left(\frac{1 + z^{-1}}{1 - B.z^{-1}}\right)$$

where

$$A = \frac{T.a}{2 + T.a}$$

$$B = \frac{2 - T.a}{2 + T.a}$$

i.e. $$H(z) = \frac{b_0 + b_1.z^{-1}}{1 - a_1.z^{-1}}$$

where

$$b_0 = A,\ b_1 = A \text{ and } a_1 = B$$

The digital filter output for the n^{th} sample, y[n], is then given in terms of the input samples x[n], etc., by:

$$y[n] = a_1.y[n-1] + b_0.x[n] + b_1.x[n-1]$$

Appendix B Rotation of Co-ordinate System

If the Cartesian co-ordinate system $\Sigma = \{0, g_1, g_2, g_3\}$ is rotated into a Cartesian coordinate system $\Sigma' = \{0, g_1', g_2', g_3'\}$, by rotating through an angle θ about an axis g through the origin, we have:

$$x' = x.[\cos(\theta) + \alpha^2.(1 - \cos(\theta)] + y.[\gamma.\sin(\theta) + \alpha.\beta.(1 - \cos(\theta))] + z.[-\beta.\sin(\theta) + \alpha.\gamma.(1 - \cos(\theta))]$$

$$y' = x.[-\gamma.\sin(\theta) + \alpha.\beta.(1 - \cos(\theta)] + y.[\cos(\theta) + \beta^2.(1 - \cos(\theta))] + z.[\alpha.\sin(\theta) + \beta.\gamma.(1 - \cos(\theta))]$$

$$z' = x.[\beta.\sin(\theta) + \alpha.\gamma.(1 - \cos(\theta)] + y.[-\alpha.\sin(\theta) + \beta.\gamma.(1 - \cos(\theta))] + z.[\cos(\theta) + \gamma^2.(1 - \cos(\theta))]$$

where x, y, z are in the system Σ and x', y', z' are in the system Σ', and α, β, γ are the direction cosines, given by:

$$\alpha = \cos\angle(g_1, g)$$

$$\beta = \cos\angle(g_2, g)$$

$$\gamma = \cos\angle(g_3, g)$$

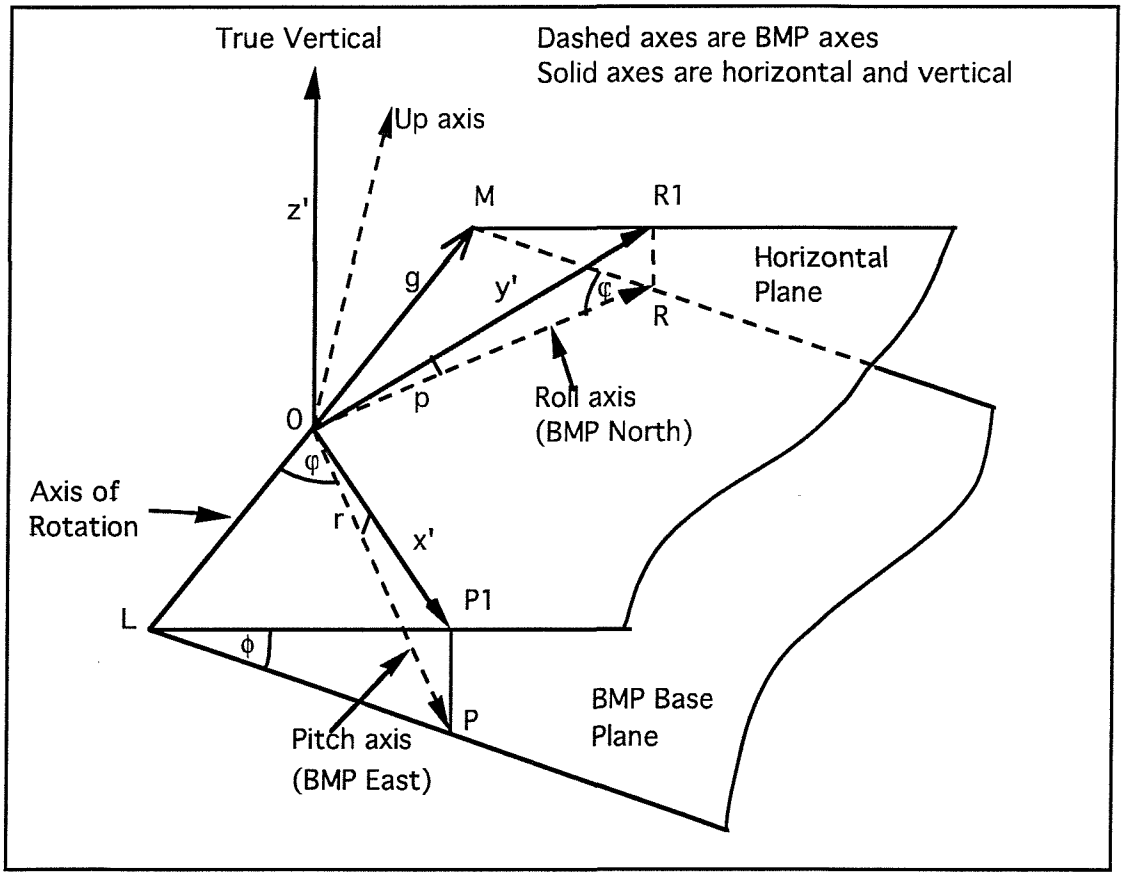

Figure A.1 BMP axis rotations

For rotation from the BMP coordinate system (g_1 = pitch axis, g_2 = roll axis, g_3 = up) to horizontal and vertical ($g_1' = x'$, $g_2' = y'$, $g_3' = z'$), we have:

$$\alpha = \cos\angle M0P = -\cos(\varphi)$$

$$\beta = \cos\angle M0R = \sin(\varphi)$$

$$\gamma = \cos\angle L0V = 0$$

and

$$\theta = -\phi \qquad \text{(since } \theta \text{ is +ve for +ve rotation about the g axis)}$$

where

$$\sin(r) = \frac{PP_1}{0P} = \left(\frac{PP_1}{LP}\right) \cdot \left(\frac{LP}{0P}\right) = \sin(\phi).\sin(\varphi)$$

$$\sin(p) = \frac{RR_1}{0R} = \left(\frac{RR_1}{MR}\right) \cdot \left(\frac{MR}{0R}\right) = \sin(\phi).\cos(\varphi)$$

so that

$$\sin(\phi) = \sqrt{\sin^2(r) + \sin^2(p)}$$

$$\cos(\phi) = \sqrt{1 - \sin^2(r) - \sin^2(p)}$$

$$\sin(\varphi) = \frac{\sin(r)}{\sqrt{\sin^2(r) + \sin^2(p)}}$$

$$\cos(\varphi) = \frac{\sin(p)}{\sqrt{\sin^2(r) + \sin^2(p)}}$$

and

$$a_{X'} = a_X.[\cos(\phi) + \cos^2(\varphi).(1 - \cos(\phi)] + a_Y.[-\sin(\varphi).\cos(\varphi).(1 - \cos(\phi)] + a_Z.[\sin(\varphi).\sin(\phi)]$$

$$a_{Y'} = a_X.[-\sin(\varphi).\cos(\varphi).(1 - \cos(\phi)] + a_Y.[\cos(\phi) + \sin^2(\varphi).(1 - \cos(\phi)] + a_Z.[\cos(\varphi).\sin(\phi)]$$

$$a_{Z'} = a_X.[-\sin(\varphi).\sin(\phi)] + a_Y.[-\cos(\varphi).\sin(\phi)] + a_Z.[\cos(\phi)]$$

Appendix C Software Descriptions

Program	Language(s)	Author	Date	Function	Section
GCMAIN3 Version 1.0	'C' and Assembler	CHC	30/03/93	BMP Firmware for SWALES	C.1
GCMAIN3T Version 2.0	'C' and Assembler	CHC	17/05/94	BMP Firmware for Calibrations	C.2
TCREAD Version 2.04	Executable File	Databook	12/03/92	Flash to Disk File transfer	C.3
Read PCMCIA vn2	QuickBasic	CHC	10/05/94	Split Flash File to binary Record Files	C.4
Decode Flash data vn2	QuickBasic	CHC	18/05/94	Convert Binary File to ASCII File	C.5
Calibrate vn7	QuickBasic	CHC	20/05/94	Convert ASCII file to Motion Data	C.6
spectrum	QuickBasic	CHC	25/05/94	Spectral Analysis of Heave, NS and EW Slopes	C.7
specrms1	QuickBasic	CHC	1/6/94	Plot Energy, Slope and Check Ratio Spectra	C.8
Direction	QuickBasic	CHC	10/06/94	Produce Directional Spectrum File	C.9
Direction1	QuickBasic	CHC	13/06/94	Produce Directional Spectrum File binned as for DWR	C.10

C.1 Acquisition Program GCMAIN3 Version 1.0

This program runs in the BMP GCAT 3000 processor. It acquires a number of 640 second records at 4 Hz sampling rate from a Young AQ wind sensor and the BMP motion/attitude sensors; the GCAT 2000 A/D convertor is used in conjunction with external multiplexors controlled by the GCAT OP2 line to give 16 channels (configured as 14 channels with offset input range).

The 81920 byte records are conditionally initiated by wind speed and the raw data are saved to Flash EEPROM memory.

The program was used for the Sonic Buoy Trials (start date 13/4/93) and for the two 1993 SWALES Deployments.

The main program is written in C (GCMAIN3.C); it uses A/D control functions in the C file GC.C and the assembler file GASM2.ASM, a Kalman filter function in GCASM.ASM and Flash Card control functions in FLASH4.ASM

These are compiled to object code files .OBJ, which are linked with the small model emulator library to produced the executable file GCMAIN3.EXE The building process is carried out by the make file G3, i.e.

```
gcmain3.exe : gcmain3.c gc.obj gasm2.obj gcasm.obj flash4.obj
        QCL /AS /Zr /c gcmain3.c
        LINK /M /ST:8000 gcmain3 gc gasm2 gcasm flash4, gcmain3.exe,,slibce.lib;
```

C.2 Calibration Program GCMAIN3T Version 2.0

This is a version of GCMAIN3 used for calibrating the sensors in the Laboratory.

It has similar analogue acquisition facilities, but without the conditional sampling and with output of 128 samples to a VDU.

The assembler functions in FLASH4.ASM are not required and the executable file is built, using the make file G3T, i.e.

```
gcmain3t.exe : gcmain3t.c gc.obj gasm2.obj gcasm.obj flash5.obj
        QCL /AS /Zr /c gcmain3t.c
        LINK /M /ST:8000 gcmain3t gc gasm2 gcasm flash5, gcmain3t.exe,,slibce.lib;
```

C.3 Recovery of Flash Card Data - 1

The Databook ThinCard drive is used to transfer the 4 Mbyte Flash Card contents to the PC hard disk file C:TEST by the simple command:

```
tcread -size 0x400000 e: c:test
```

For transfer to Macintosh by floppy disk, this file is then split into 4 x 1 Mbyte files by the PC application 4MTO1M.EXE and the floppy files are then recombined into the 4 Mbyte file BMPSWAL.ALL, using Word on the Macintosh.

C.4 Recovery of Flash Card Data - 2

The 4 Mbyte file is then split into the individual 81920 byte records, using the "directory" information in the first 256 kbytes of the file; this process is carried out by the simple QuickBasic application "Read PCMCIA vn2". The resultant binary files are named BMPjjjhh, where jjj is the Julian day and hh are the hours of the record start time. The files consist, nominally, of 2560 scans, each of 16 channels, where each channel is 2 byte binary (least significant byte first).

C.5 Decoding Flash Card Files - 1

The QuickBasic program "Decode Flash data vn2" is first used to convert the binary BMPjjjhh files to decimal integer ASCII files BMPjjjhhdec. The files consist, nominally, of 2560 scans, each of 16 channels, where each channel has the format +NNNN (range -4096 to +4095). Channels are separated by commas (character 44) and scans are separated by carriage returns (character 13)

C.6 Decoding Flash Card Files - 2

The QuickBasic program "Calibrate vn7" is then used to convert the ASCII data to calibrated buoy motion data, consisting of 3 components of displacement and the NS and EW slopes.

The time series of these 5 variables are saved in the files BMPjjjhhcal, each sample having the format:

+z.zzzzE+zz<tab>+x.xxxxE+xx<tab>+y.yyyyE+yy<tab>+n.nnnnE+nn<tab>+e.eeeeE+ee<CR>

C.7 Spectral Analysis

The QuickBasic program "spectrum" is used to carry out 2048 point spectral analyses of the vertical displacement and slope times series files BMPjjjhhcal, resulting in BMPjjjhhspec output files of the 2048 complex estimates, with each set of complex estimates, n, having the format:

+z.zzzzE+zz,+n.nnnnE+nn,+e.eeeeE+ee<CR> (real components, r(m,n))

+z.zzzzE+zz,+n.nnnnE+nn,+e.eeeeE+ee<CR> (imaginary components, i(m,n))

i.e.

r(1,n),r(2,n),r(3,n)<CR>

i(1,n),i(2,n),i(3,n)<CR>

The first 400 samples of the 2560 sample files are skipped, so as to miss out the digital filter transients.

C.8 Spectral Display

The QuickBasic program "specrms1" can be used to derive the significant wave height and zero-crossing period and to display the energy spectrum, slope spectrum and check ratio.

The significant wave height, Hs, is calculated from the zero order moment of the heave spectrum, m_o, as follows:

$$Hs = 4.\sqrt{m_o}\text{, where } m_o = \sum_{n=1}^{2047}\left(r(^2 1,n) + i^2(1,n)\right)$$

The zero-crossing period, Tz, is calculated from the zero and second order moments, m_o and m_2, as follows:

$$Tz = \sqrt{\frac{m_o}{m_2}}, \text{ where } \quad m_2 = \sum_{n=1}^{2047} \left(r^2(1,n) + i^2(1,n) \right) \cdot f_n^2$$

and the frequency of the estimate, $f_n = \frac{n}{512}$ Hz n=1 to 1024

$f_n = \frac{2048 - n}{512}$ Hz n=1024 to 2047

Smoothed heave energy, equivalent slope energy and check ratio spectra are plotted, using bins of 8 estimates. The equivalent slope energy in metres^2 is given by the slope energy (in rad^2) divided by the square of the wave number, k.

A 5th order fit was used to derive the wave number, k, in terms of angular frequency, Ω, from the shallow wave dispersion relationship:

$\Omega^2 = g.k.\tanh(kD)$, where $g = 9.81$ ms^{-2} and D is the depth in metres (50)

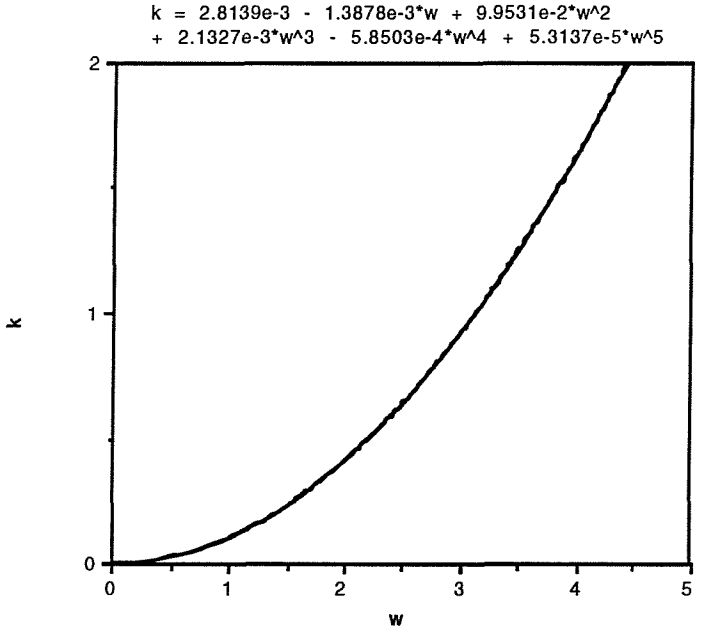

Figure C.1 Plot of Wave number, k, against Angular Frequency, ω, for 50 metre depth

The computed fit was:

$k = 2.8139E\text{-}03 - 1.3878E\text{-}03*\omega + 9.9531E\text{-}2*\omega^2 + 2.1327E\text{-}3*\omega^3 - 5.8503E\text{-}4*\omega^4 + 5.3137E\text{-}5*\omega^5$

$$\text{Heave energy } C_{11}(\text{bin\%}) = \sum_{n=n_{min}(\text{bin\%})}^{n_{max}(\text{bin\%})} \left(r^2(1,n) + i^2(1,n) \right) \quad \text{metres}^2$$

$$\text{Slope energy} = \frac{C_{22}(\text{bin\%}) + C_{33}(\text{bin\%})}{k^2} \quad \text{metres}^2$$

where

$$C_{22}(\text{bin\%}) = \sum_{n = n_{min}(\text{bin\%})}^{n_{max}(\text{bin\%})} \left(r^2(2,n) + i^2(2,n) \right)$$

$$C_{33}(\text{bin\%}) = \sum_{n = n_{min}(\text{bin\%})}^{n_{max}(\text{bin\%})} \left(r^2(3,n) + i^2(3,n) \right)$$

$$\text{Check Ratio } R = \frac{\text{Heave energy}}{\text{Slope energy}}$$

C.9 Directional Analysis - 1

Two versions of QuickBasic directional analysis program can then be used with the BMPjjjhhspec files; the first form, "Direction", results in BMPjjjhhspecd files with 64 smoothed (binned) estimates of the form:

f(bin%)<TAB>C_{11}(bin%)<TAB>θ_1(bin%)<TAB>θ_2(bin%)

where f(bin%) runs from 8/1024 Hz to 1016/1024 Hz in steps of 16/1024 (spectral estimate width 16/1024 Hz). The parameters C_{11}(bin%), θ_1(bin%) and θ_2(bin%) are, respectively, the spectral energy density, mean direction and directional spread.

C.10 Directional Analysis - 2

The second form, "Direction1", results in a directional spectrum binned in the same frequency bins as the corresponding DWRjjj.jjjj file (where jjj.jjjj is jjj + hh/24 expressed in 4 digit decimal form). This results in 15 estimates of the form:

f(bin%)<TAB>C_{11}(bin%)<TAB>θ_1(bin%)<TAB>θ_2(bin%)<TAB>θ_{12}(bin%)<TAB>θ_{12}'(bin%)

where bin% is the bin number, θ_{12} and θ_{12}' are alternative values of θ_1 derived from the second harmonic terms in the directional expansion. These estimates are output to a BMPjjjhhspecd1 file with a header in a suitable form to produce a block graph in Cricket Graph.

The directional spectra are obtained from the complex estimates produced by the application "spectrum", using the standard technique (ref. 3) as follows:

For a given estimate, n, the complex estimates are read from the BMPjjjhhspec file in the order:

r(1,n), r(2,n), r(3,n)

i(1,n), i(2,n), i(3,n)

where series 1 is heave, series 2 is NS slope and series 3 is EW slope.

The required smoothed co- and quad spectral estimates are formed by binning the products as follows:

$$C_{11}(\text{bin\%}) = \sum_{n=n_{min}(\text{bin\%})}^{n_{max}(\text{bin\%})} \left(r^2(1,n) + i^2(1,n)\right)$$

$$C_{22}(\text{bin\%}) = \sum_{n=n_{min}(\text{bin\%})}^{n_{max}(\text{bin\%})} \left(r^2(2,n) + i^2(2,n)\right)$$

$$C_{33}(\text{bin\%}) = \sum_{n=n_{min}(\text{bin\%})}^{n_{max}(\text{bin\%})} \left(r^2(3,n) + i^2(3,n)\right)$$

$$Q_{12}(\text{bin\%}) = \sum_{n=n_{min}(\text{bin\%})}^{n_{max}(\text{bin\%})} \left(i(1,n).r(2,n) - r(1,n).i(2,n)\right)$$

$$Q_{13}(\text{bin\%}) = \sum_{n=n_{min}(\text{bin\%})}^{n_{max}(\text{bin\%})} \left(i(1,n).r(3,n) - r(1,n).i(3,n)\right)$$

$$C_{23}(\text{bin\%}) = \sum_{n=n_{min}(\text{bin\%})}^{n_{max}(\text{bin\%})} \left(r(2,n).r(3,n) + i(2,n).i(3,n)\right)$$

where bin% runs from 1 to 64 and $n_{max} = 16*(\text{bin\%})$, $n_{min} = 16*(\text{bin\%}-1)$ in the application Direction and

where bin% runs from 1 to 15 and n_{max}, n_{min} are dependent upon the DWR frequency bins in the application Direction1

The binned co- and quad spectral estimates are then converted to engineering units of m^2/Hz or rad^2/Hz or m*rad/Hz

The normalised complex angular harmonic components, A_1, B_1, A_2 and B_2, for each bin are then calculated from:

$$A_1(\text{bin\%}) = \frac{Q_{12}(\text{bin\%})}{\sqrt{C_{11}(\text{bin\%}).(C_{22}(\text{bin\%}) + C_{33}(\text{bin\%}))}}$$

$$B_1(\text{bin\%}) = \frac{Q_{13}(\text{bin\%})}{\sqrt{C_{11}(\text{bin\%}).(C_{22}(\text{bin\%}) + C_{33}(\text{bin\%}))}}$$

$$A_2(\text{bin\%}) = \frac{C_{22}(\text{bin\%}) - C_{33}(\text{bin\%})}{C_{22}(\text{bin\%}) + C_{33}(\text{bin\%})}$$

$$B_2(\text{bin\%}) = \frac{2*C_{23}(\text{bin\%})}{C_{22}(\text{bin\%}) + C_{33}(\text{bin\%})}$$

Assuming a unimodal directional distribution of the form:

$$G(\theta) \approx \cos^{2s}(0.5*(\theta - \theta_1))$$

the mean direction, spread parameter and the directional spread can then be derived from the 1st order components, A_1 and B_1, or from the 2nd order components, A_2 and B_2.

From the 1st order components:

$$\text{Mean wave direction, } \theta_1(\text{bin\%}) = \arctan\left(\frac{B_1(\text{bin\%})}{A_1(\text{bin\%})}\right)$$

$$\text{Spread Parameter, } s_1(\text{bin\%}) = \frac{C_1(\text{bin\%})}{1 - C_1(\text{bin\%})}$$

$$\text{where } C_1(\text{bin\%})^2 = A_1(\text{bin\%})^2 + B_1(\text{bin\%})^2$$

$$\text{Directional Spread, } \theta_2(\text{bin\%}) = \sqrt{\frac{2}{s_1(\text{bin\%}) + 1}}$$

From the 2nd order components:

$$\text{Mean wave direction, } \theta_{12}(\text{bin\%}) = 0.5*\arctan\left(\frac{B_2(\text{bin\%})}{A_2(\text{bin\%})}\right)$$

$$\text{Spread Parameter, } s_2(\text{bin\%}) = \frac{1 + 3*C_2(\text{bin\%}) + \sqrt{1 + 14*C_2(\text{bin\%}) + C_2(\text{bin\%})^2}}{2*(1 - C_2(\text{bin\%}))}$$

$$\text{where } C_2(\text{bin\%})^2 = A_2(\text{bin\%})^2 + B_2(\text{bin\%})^2$$

$$\text{Directional Spread, } \theta_2(\text{bin\%}) = \sqrt{\frac{2}{s_2(\text{bin\%}) + 1}}$$

Note that, in the case of θ_{12}, it may necessary to add π radians on inspection, since the factor of 0.5 gives results directly only in the range $-\pi/2$ to $+\pi/2$.

Appendix D Summary of Parameterised Data

Date	BMP Hs (m)	DWR Hs (m)	BMP Tz (s)	DWR Tz (s)	BMP Direction (pk)	DWR Direction (pk)	BMP Spread (pk)	DWR Spread (pk)
293.625	0.84	0.85	4.32	4.46	306.1	275.6	37.2	24.6
293.750	0.75	0.80	3.33	3.06	279.8	264.4	52.8	35.7
294.000	0.98	1.05	4.05	3.72	276.5	281.2	34.5	20.0
294.125	1.03	1.15	4.44	4.14	215.1	258.8	69.4	29.8
294.250	1.01	1.05	4.19	3.85	301.8	247.5	46.8	35.7
294.375	0.86	0.85	5.08	3.99	230.2	253.1	62.2	35.7
294.500	0.84	0.99	3.71	3.85	202.5	241.9	71.4	24.6
294.625	1.05	1.21	3.85	3.72	288.4	253.1	68.3	24.6
306.500	1.23	1.52	3.75	3.85	102.0	106.9	40.6	24.6
306.625	1.50	1.52	4.57	4.63	104.3	106.9	36.5	20.0
306.750	1.95	1.66	5.46	5.01	85.8	101.2	35.7	24.6
306.875	2.04	1.74	4.71	4.14	98.4	106.9	41.3	24.6
307.000	1.70	1.81	4.25	4.29	120.8	106.9	54.5	24.6
307.125	1.66	1.66	4.94	4.82	104.3	112.5	34.2	20.0
313.375	2.04	2.32	4.92	4.82	265.9	247.5	48.0	24.6
313.500	3.11	2.93	5.84	5.45	273.3	258.8	26.4	24.6
327.375	1.05	1.10	5.29	4.63	294.0	258.8	31.3	29.8
327.625	1.31	1.27	4.91	4.14	240.5	258.8	51.5	29.8
327.750	1.38	1.39	4.63	3.99	217.9	264.4	33.3	29.8
327.875	1.55	1.46	5.05	4.29	153.4	118.1	49.0	49.9
328.000	1.75	1.81	5.32	4.82	148.9	123.8	55.6	42.3
328.125	2.24	2.14	5.31	4.63	142.1	135.0	47.3	42.3
328.250	2.37	2.41	5.23	4.82	165.7	146.2	41.8	42.3
328.375	3.18	2.93	5.88	5.45	157.9	140.6	45.6	29.8
328.500	3.06	2.71	5.87	5.23	181.9	140.6	22.0	35.7
328.625	2.31	2.23	5.24	4.82	168.1	135.0	56.0	42.3
328.750	2.56	2.82	6.18	5.95	239.0	247.5	14.9	16.0
328.875	3.12	3.40	6.44	6.24	282.9	258.8	30.6	16.0
329.000	2.60	2.93	6.15	5.95	284.3	270.0	26.1	20.0
331.875	2.46	2.23	4.99	4.63	203.7	258.8	66.3	29.8
332.250	2.69	2.93	5.33	5.45	87.6	106.9	40.2	29.8
332.375	2.76	2.93	5.53	5.45	108.1	112.5	50.5	24.6
332.500	3.31	3.16	6.58	5.69	113.0	112.5	22.4	24.6
332.625	3.05	3.40	6.57	6.24	120.7	106.9	47.0	29.8
332.750	3.39	3.40	6.02	5.69	111.4	112.5	40.4	29.8
332.875	3.34	3.16	5.78	5.69	116.6	112.5	29.1	20.0
333.000	2.63	3.16	6.23	5.69	120.7	123.8	45.4	29.8

Appendix E Comparison of BMP and DWR Directional Spectra obtained during SWALES 1st and 2nd Deployments

The BMP and DWR Energy Density, Direction from and Spread spectra for all of the BMP records are shown in figures E.1a-c to E.37a-c.

Figures E.1a-c 29315 Directional Spectrum

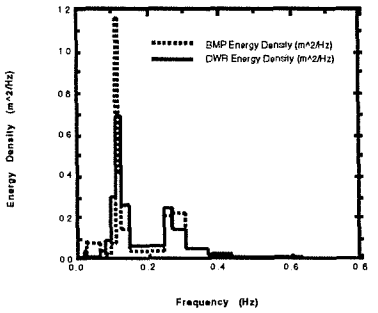

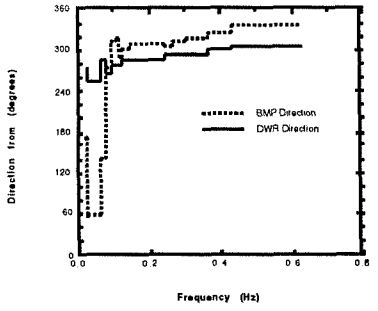

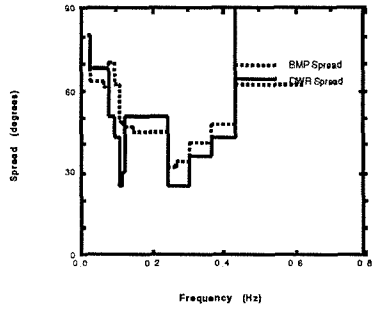

Figures E.2a-c 29318 Directional Spectrum

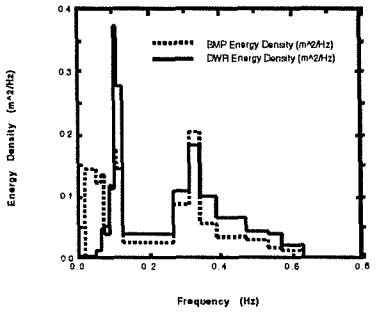

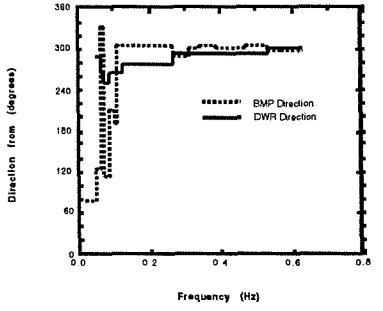

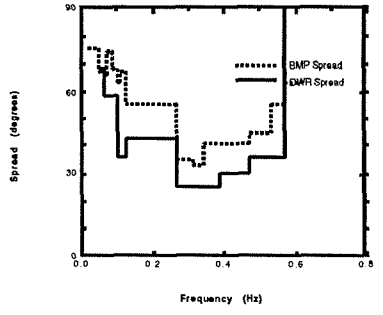

Figures E.3a-c 29400 Directional Spectrum

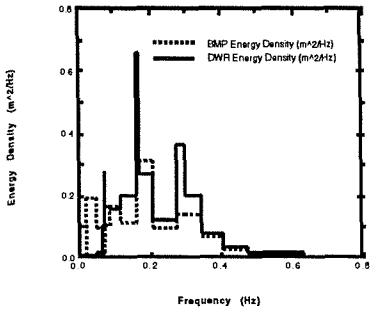

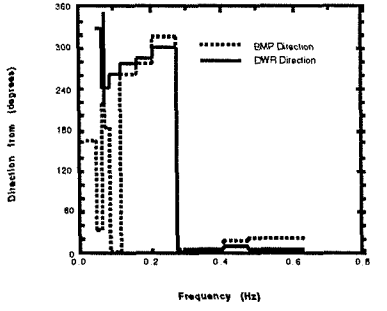

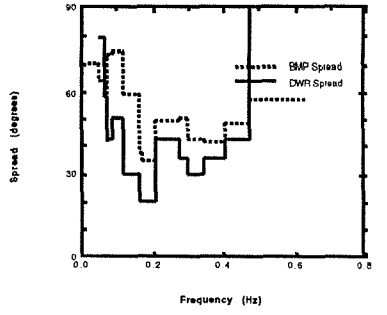

Figures E.4a-c 29403 Directional Spectrum

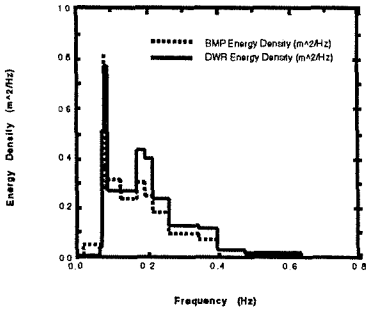

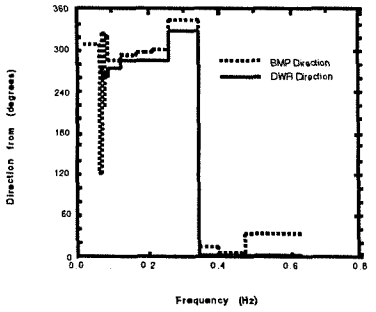

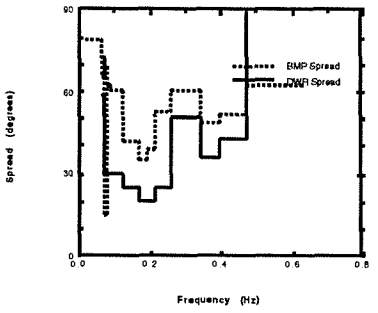

Figures E.5a-c 29406 Directional Spectrum

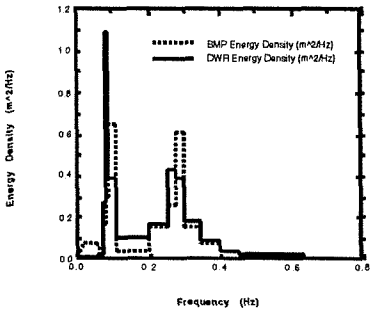

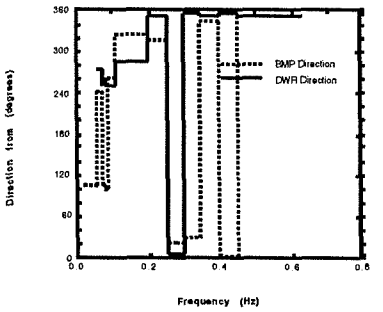

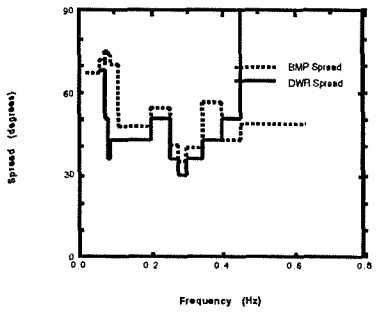

Figures E.6a-c 29409 Directional Spectrum

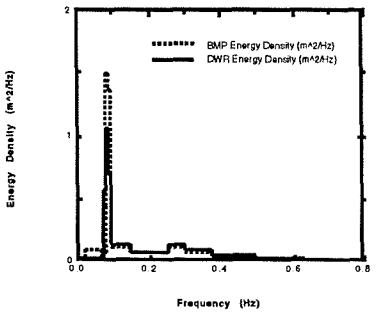

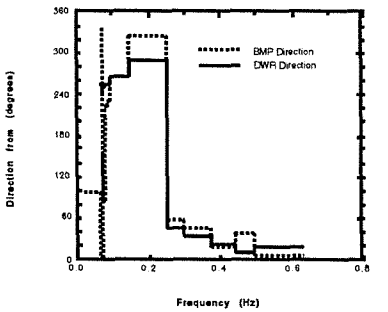

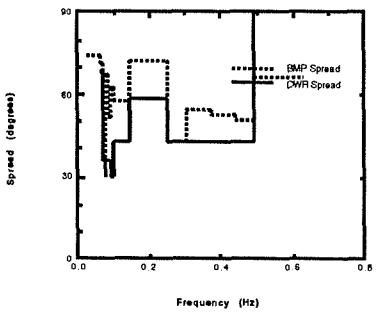

Figures E.7a-c 29412 Directional Spectrum

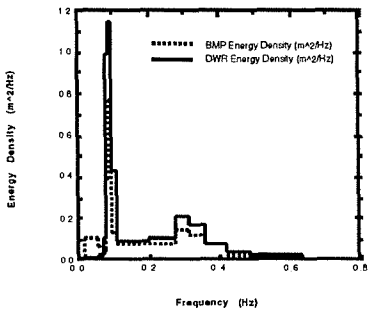

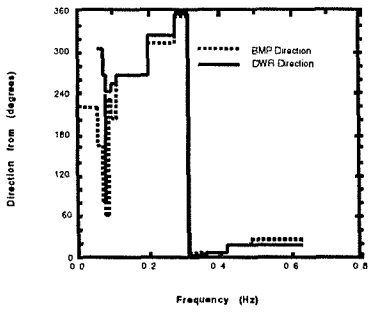

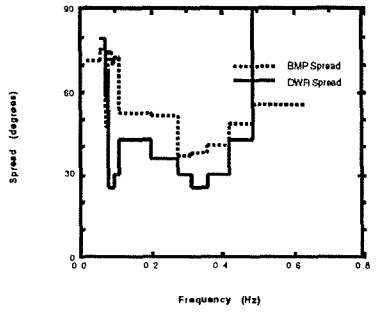

Figures E.8a-c 29415 Directional Spectrum

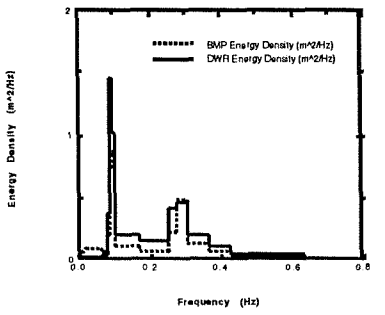

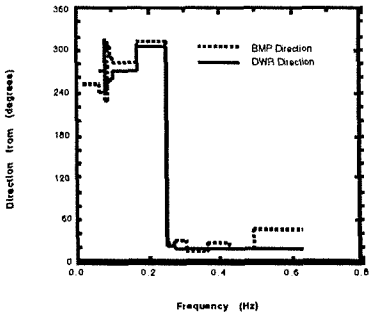

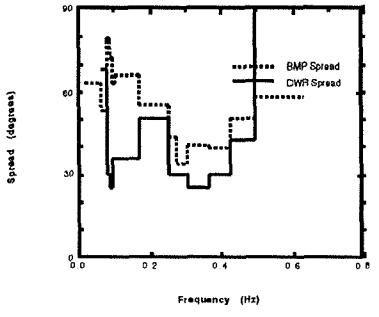

Figures E.9a-c 30612 Directional Spectrum

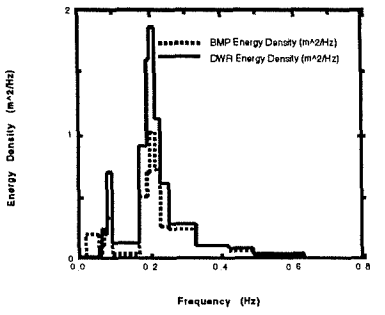

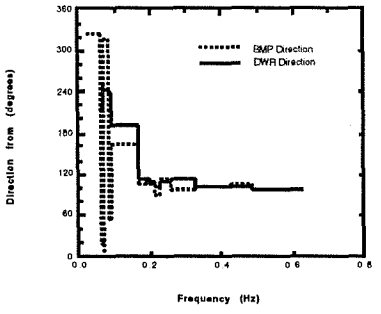

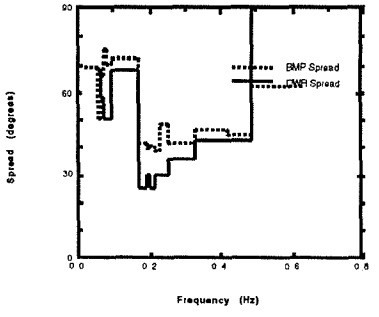

Figures E.10a-c 30615 Directional Spectrum

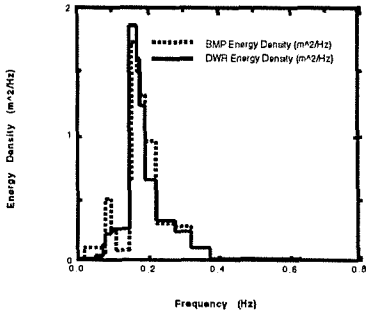

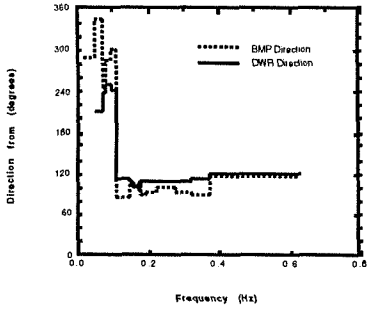

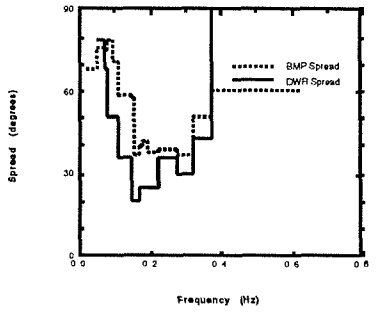

Figures E.11a-c 30618 Directional Spectrum

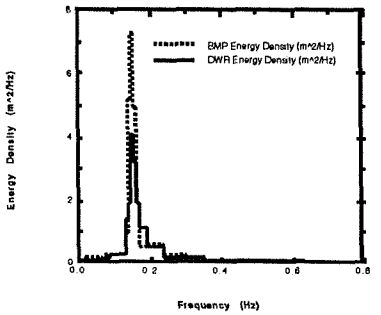

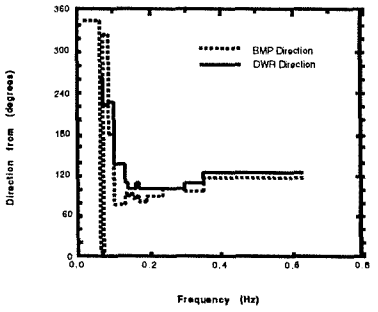

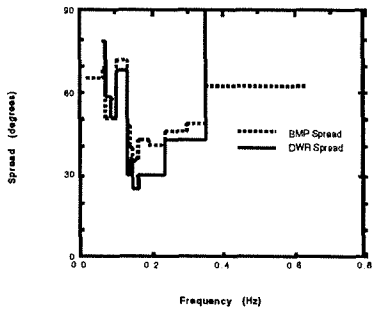

Figures E.12a-c 30621 Directional Spectrum

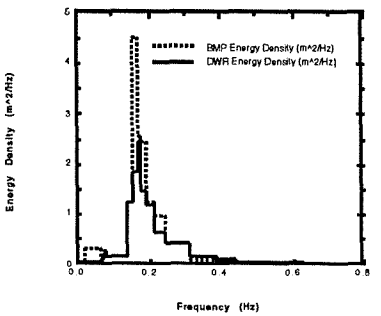

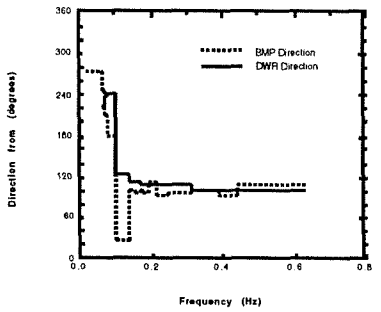

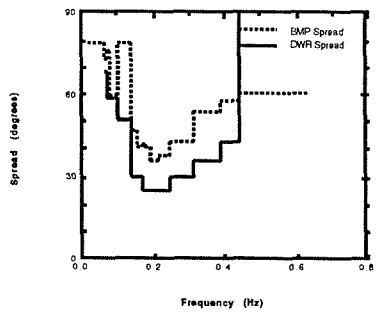

Figures E.13a-c 30700 Directional Spectrum

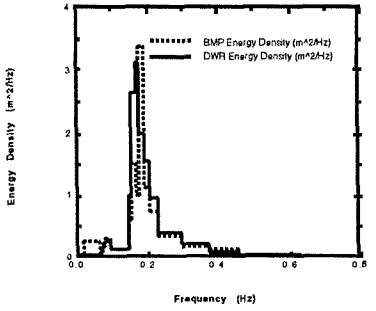

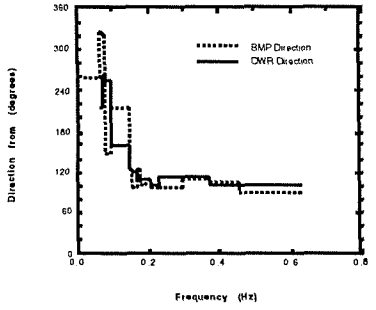

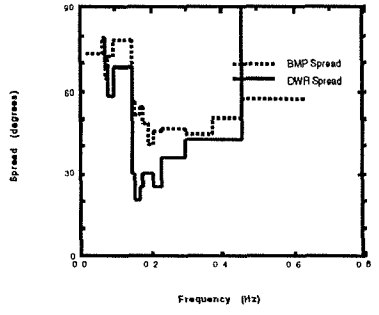

Figures E.14a-c 30703 Directional Spectrum

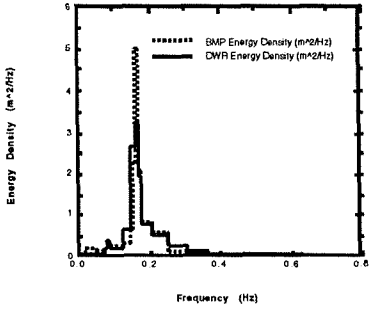

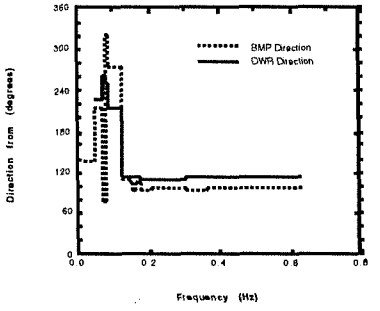

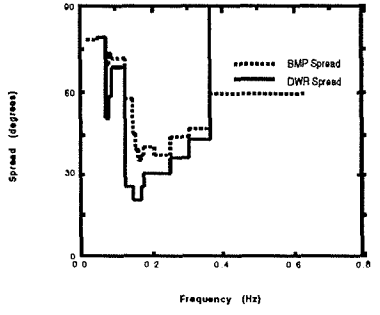

Figures E.15a-c 31309 Directional Spectrum

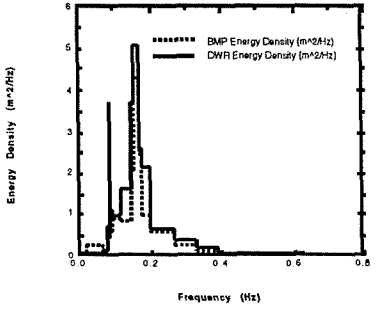

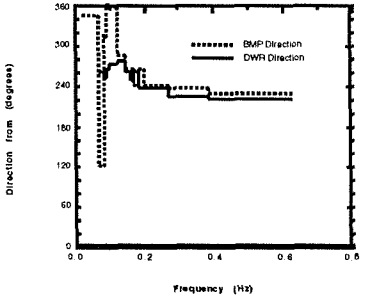

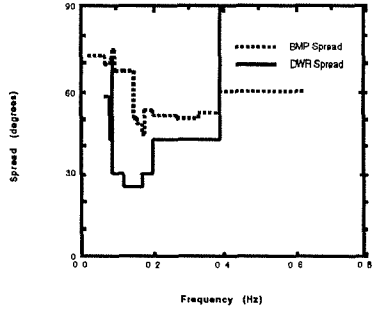

Figures E.16a-c 31312 Directional Spectrum

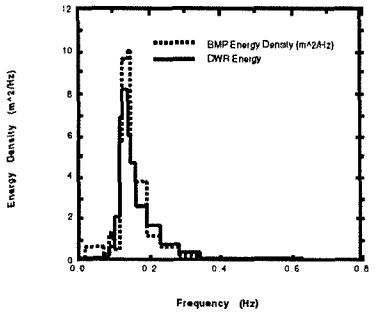

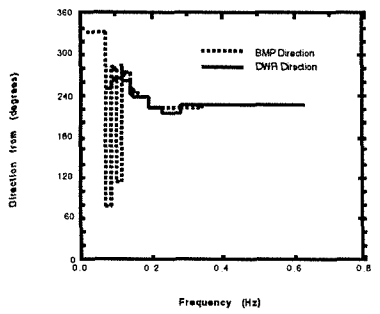

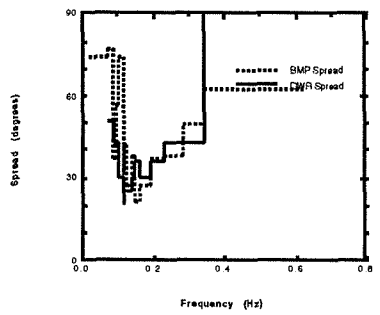

Figures E.17a-c 32709 Directional Spectrum

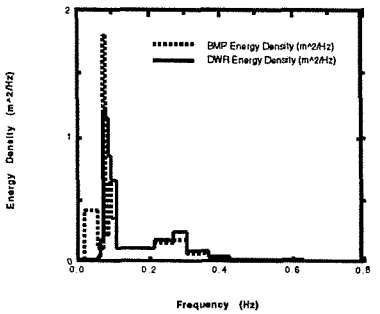

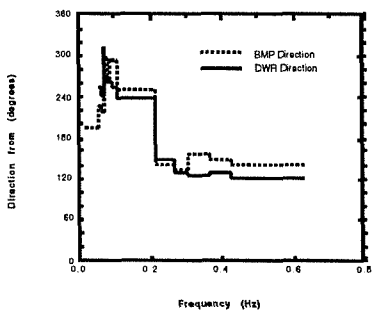

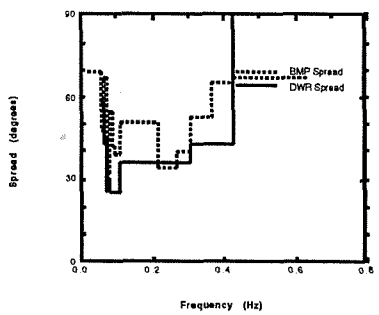

Figures E.18a-c 32715 Directional Spectrum

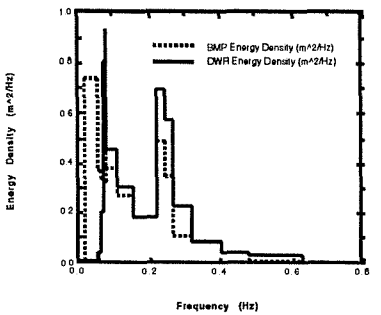

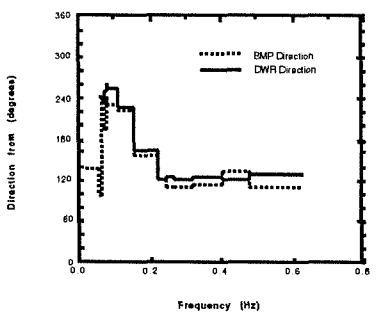

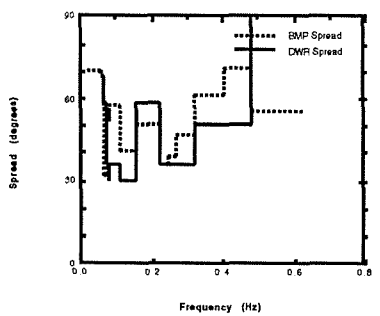

Figures E.19a-c 32718 Directional Spectrum

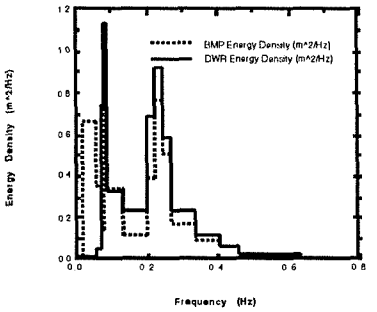

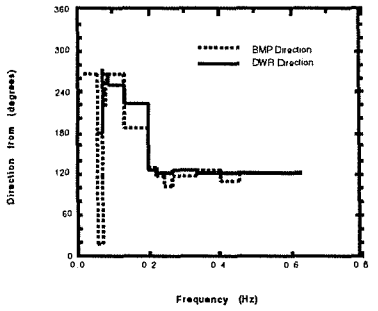

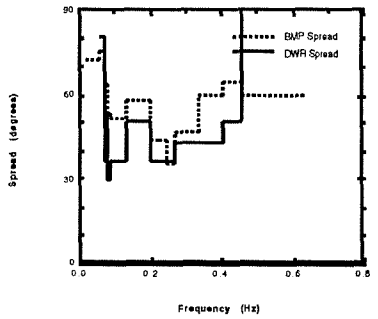

Figures E.20a-c 32721 Directional Spectrum

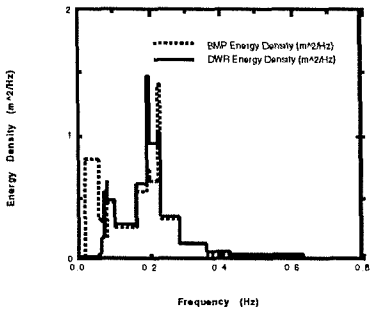

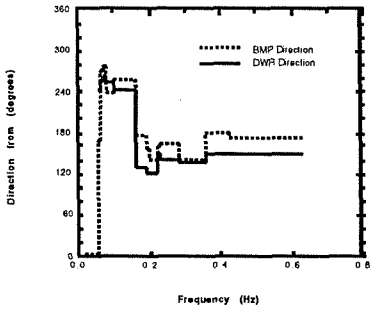

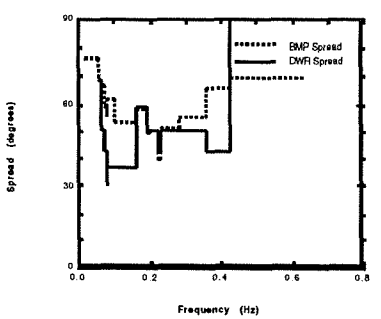

Figures E.21a-c 32800 Directional Spectrum

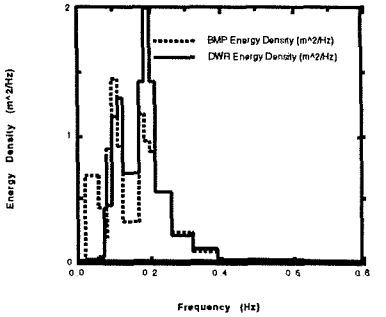

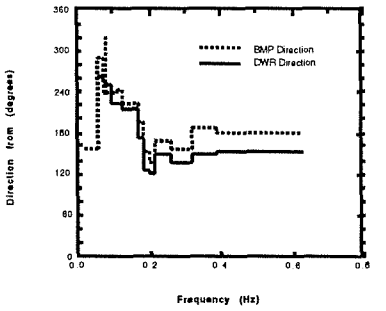

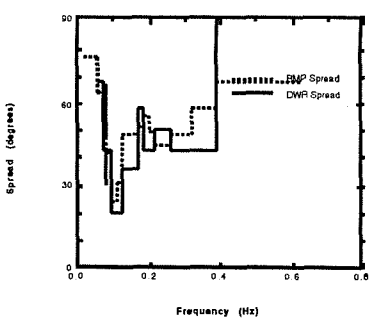

Figures E.22a-c 32803 Directional Spectrum

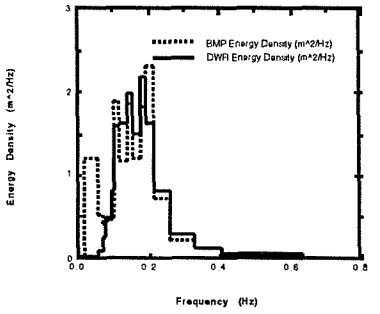

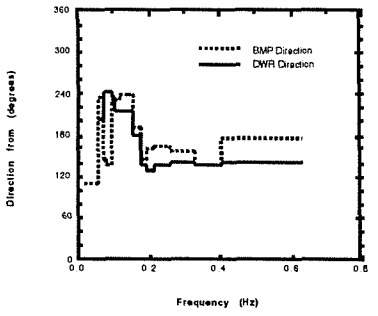

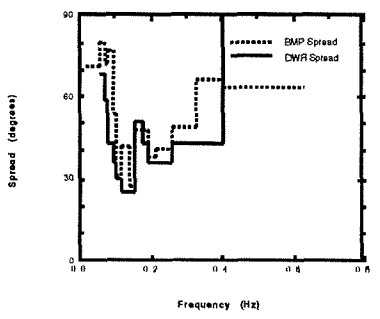

Figures E.23a-c 32806 Directional Spectrum

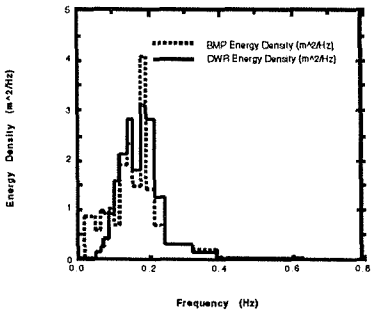

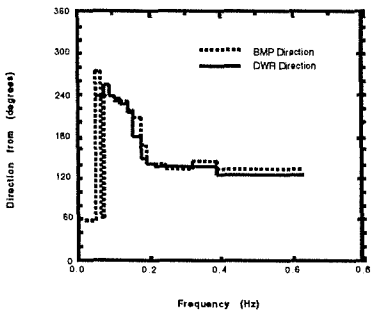

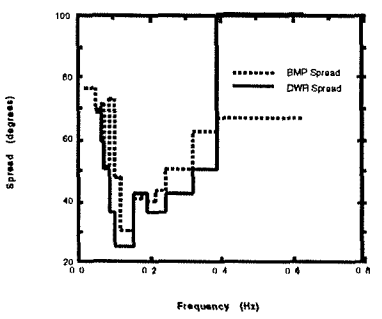

Figures E.24a-c 32809 Directional Spectrum

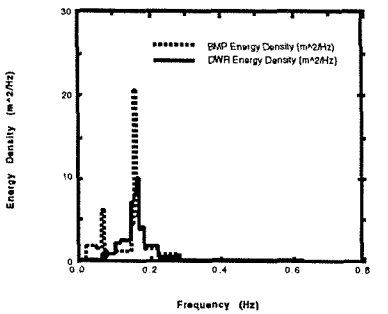

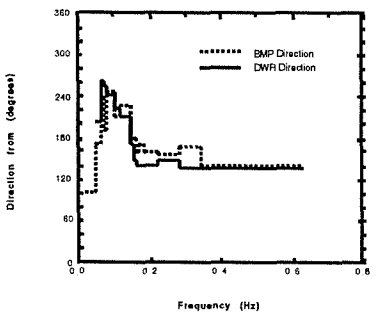

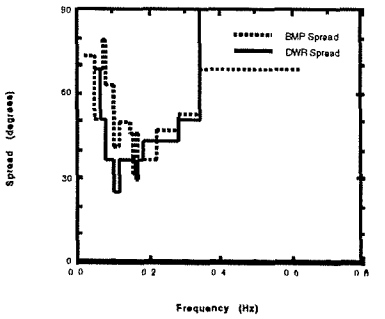

Figures E.25a-c 32812 Directional Spectrum

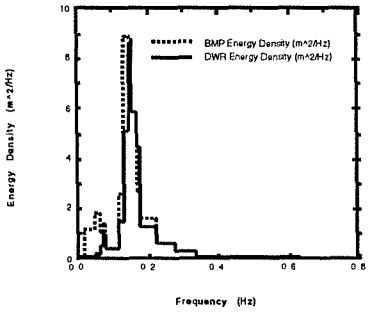

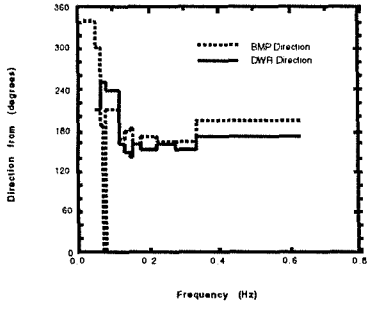

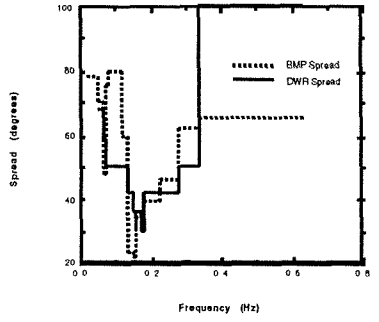

Figures E.26a-c 32815 Directional Spectrum

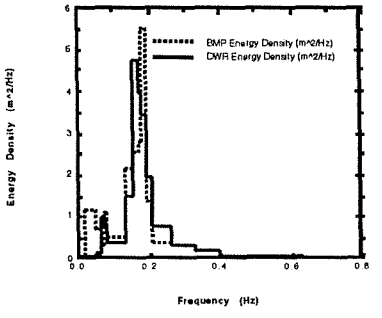

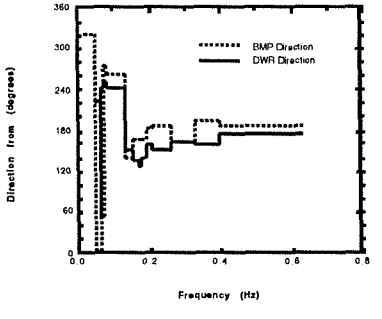

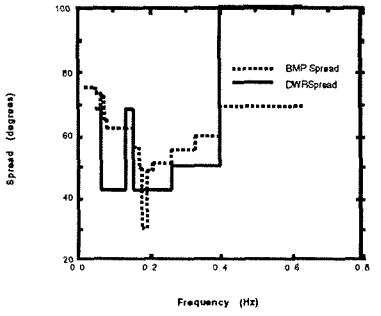

Figures E.27a-c 32818 Directional Spectrum

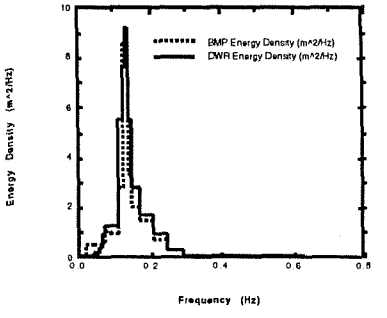

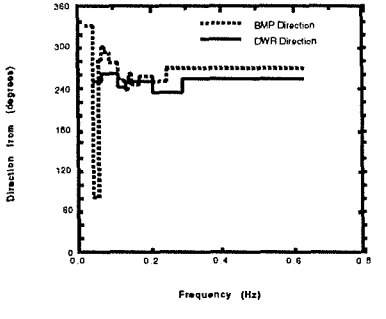

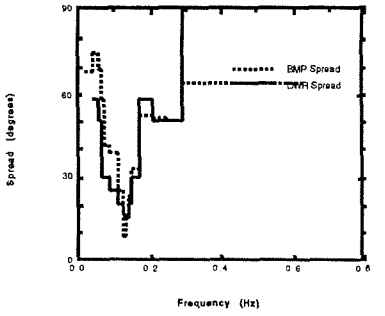

Figures E.28a-c 32821 Directional Spectrum

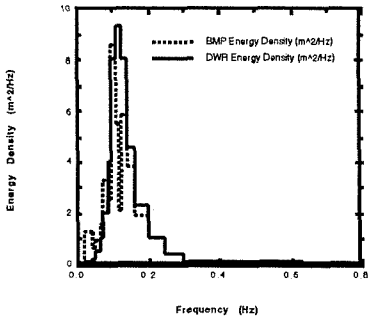

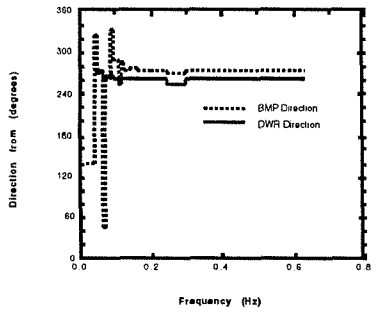

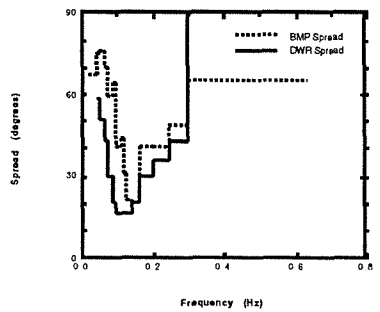

Figures E.29a-c 32900 Directional Spectrum

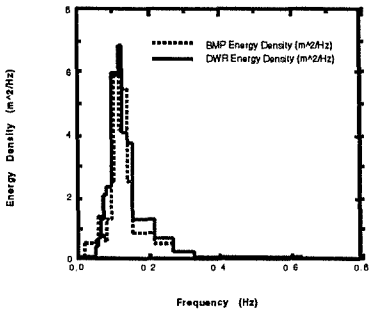

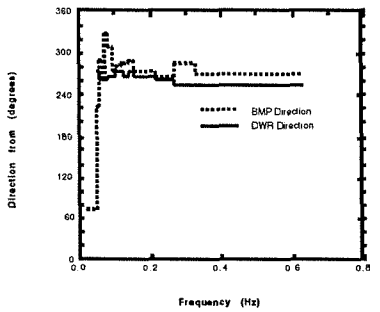

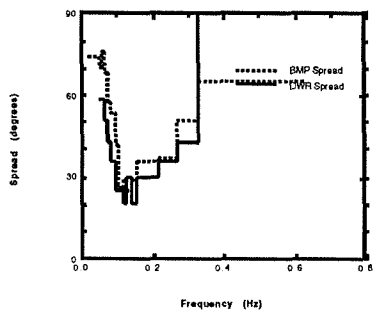

Figures E.30a-c 33121 Directional Spectrum

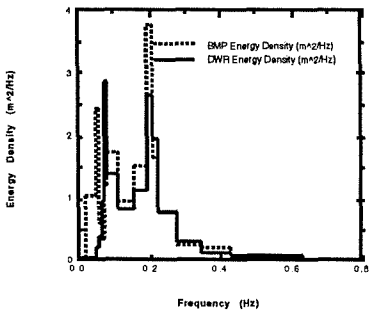

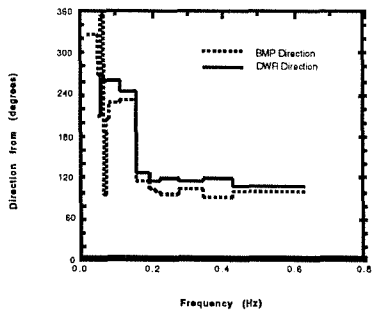

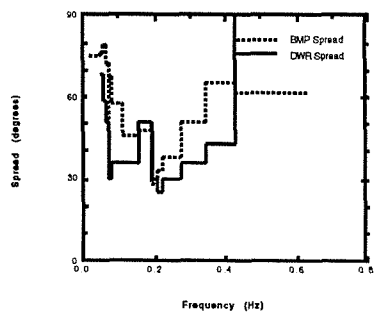

Figures E.31a-c 33206 Directional Spectrum

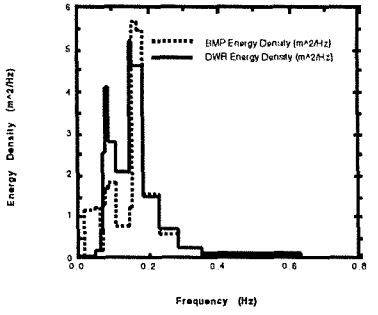

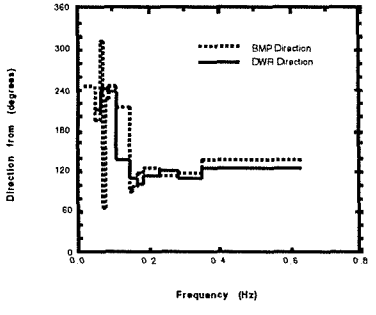

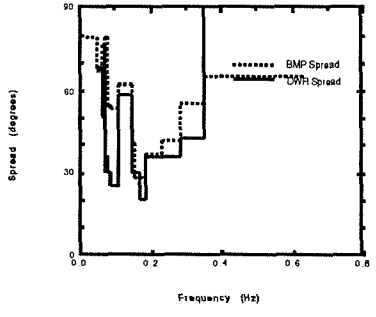

Figures E.32a-c 33209 Directional Spectrum

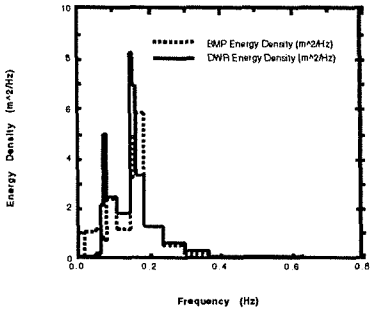

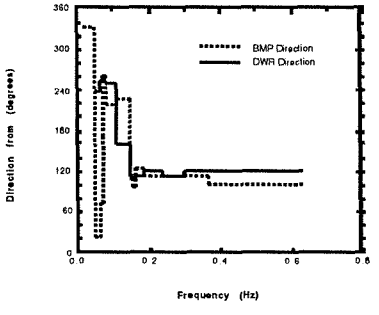

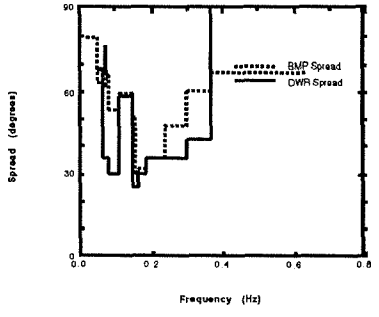

Figures E.33a-c 33212 Directional Spectrum

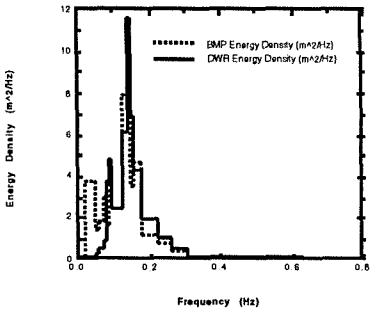

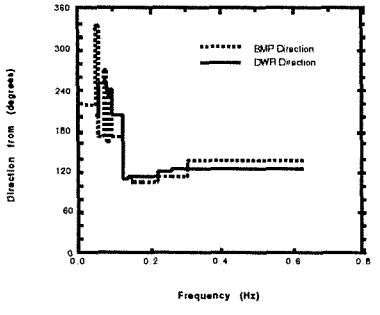

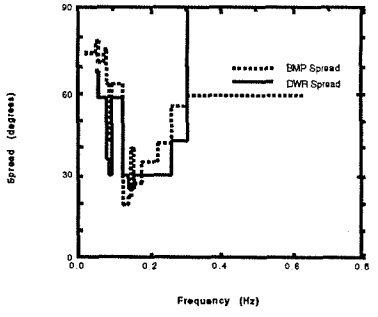

Figures E.34a-c 33215 Directional Spectrum

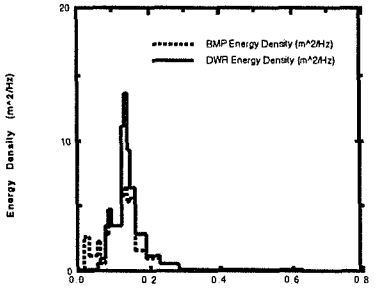

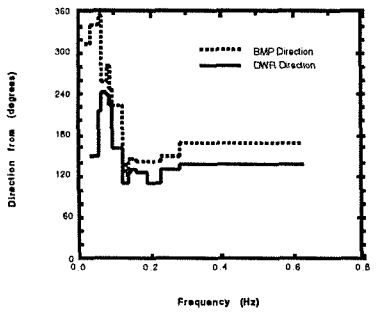

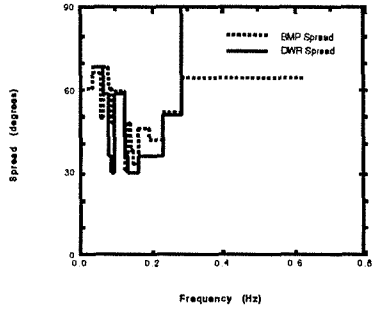

Figures E.35a-c 33218 Directional Spectrum

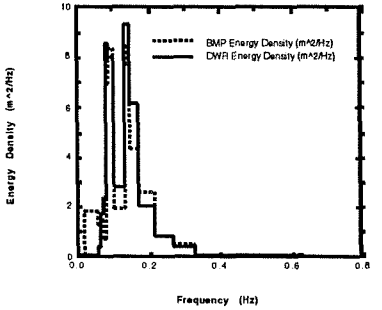

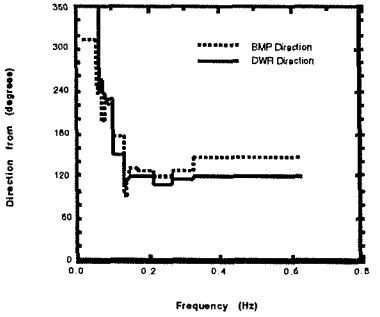

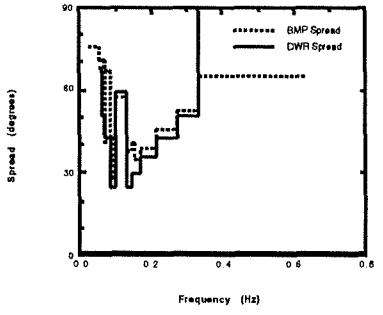

Figures E.36a-c 33221 Directional Spectrum

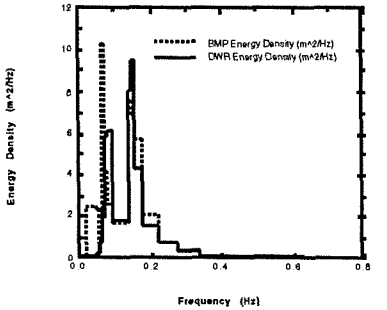

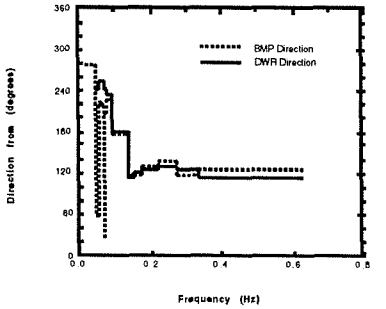

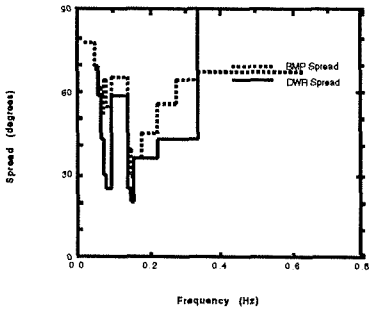

Figures E.37a-c 33300 Directional Spectrum